iScience

CellPress

Article

MicroRNA miR-1002 Enhances NMNAT-Mediated Stress Response by Modulating Alternative Splicing

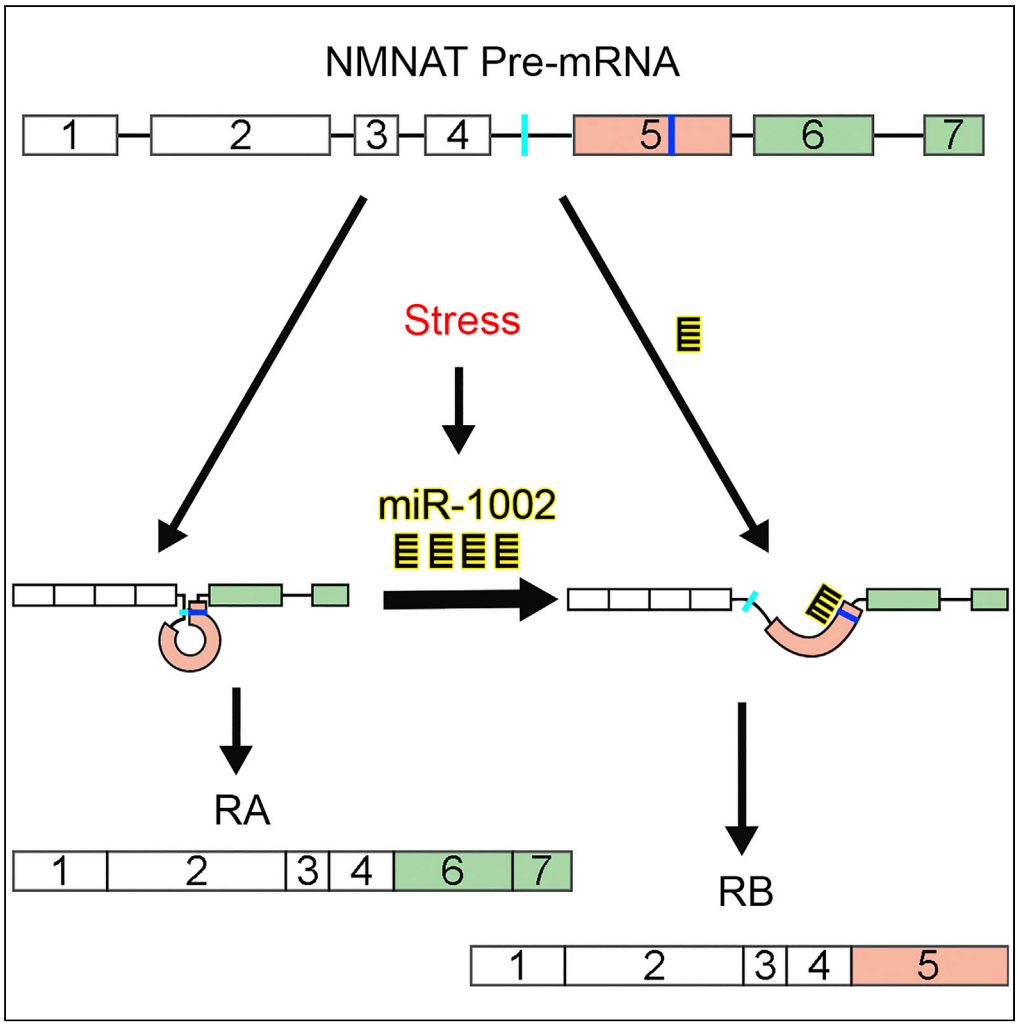

Joun Park, Yi Zhu, Xianzun Tao, Jennifer M. Brazill, Chong Li, Stefan Wuchty, R. Grace Zhai

gzhai@med.miami.edu

HIGHLIGHTS

miR-1002 regulates splicing of NMNAT pre-mRNA

miR-1002 binding facilitates the splicing of neuroprotective NMNAT isoform

Stress upregulates miR-1002 and enhances NMNAT-mediated neuroprotection

Argonaute 1 is involved in miR-1002-mediated regulation of NMNAT splicing

Park et al., iScience *19*, 1048–1064
September 27, 2019 © 2019 The Author(s).
https://doi.org/10.1016/j.isci.2019.08.052

iScience

CellPress

Article

MicroRNA miR-1002 Enhances NMNAT-Mediated Stress Response by Modulating Alternative Splicing

Joun Park,[1,2] Yi Zhu,[1,3] Xianzun Tao,[1] Jennifer M. Brazill,[1,3,6] Chong Li,[1,4,7] Stefan Wuchty,[5] and R. Grace Zhai[1,2,3,4,8,*]

SUMMARY

Understanding endogenous regulation of stress resistance and homeostasis maintenance is critical to developing neuroprotective therapies. Nicotinamide mononucleotide adenylyltransferase (NMNAT) is a conserved essential enzyme that confers extraordinary protection and stress resistance in many neurodegenerative disease models. *Drosophila Nmnat* is alternatively spliced to two mRNA variants, RA and RB. RB translates to protein isoform PD with robust protective activity and is upregulated upon stress to confer enhanced neuroprotection. The mechanisms regulating the alternative splicing and stress response of NMNAT remain unclear. We have discovered a *Drosophila* microRNA, *dme-miR-1002*, which promotes the splicing of NMNAT pre-mRNA to RB by disrupting a pre-mRNA stem-loop structure. NMNAT pre-mRNA is preferentially spliced to RA in basal conditions, whereas miR-1002 enhances NMNAT PD-mediated stress protection by binding via RISC component Argonaute1 to the pre-mRNA, facilitating the splicing switch to RB. These results outline a new process for microRNAs in regulating alternative splicing and modulating stress resistance.

INTRODUCTION

Neuronal stress resistance is a critical component of health and activity. For many animals, neurons produced during development cannot be replaced and must last for the lifetime of the organism (Asatryan and Bazan, 2017). These neurons withstand a plethora of cellular stressors to maintain viability in the face of disease (Orsini et al., 2016), environmental afflictions (Kagias et al., 2012; Kim and Jin, 2015; Saxena and Caroni, 2011), and aging (Chandra et al., 2017; Chandran et al., 2017; Kirkwood, 2003). Understanding how neurons combat stress has wide-ranging implications for organismal health and quality of life.

Nicotinamide mononucleotide adenylyltransferase (NMNAT) is a housekeeping enzyme responsible for the synthesis of nicotinamide adenine dinucleotide (NAD^+) in all living organisms (Zhai et al., 2009). In addition, NMNAT proteins are essential for neuronal maintenance and protection (Ali et al., 2012; Brazill et al., 2017; Fang et al., 2012; Kitaoka et al., 2013; Press and Milbrandt, 2008; Rossi et al., 2018; Sasaki and Milbrandt, 2010; Sasaki et al., 2009; Wen et al., 2011; Yan et al., 2010; Zhai et al., 2006, 2008). NMNAT has been shown to confer robust resistance against various stressors across many species, including hypoxia (Ali et al., 2011; Wen et al., 2013), heat (Ali et al., 2011), oxidative stress (Chiurchiù et al., 2016; Cobley et al., 2018), disease states (Ali et al., 2012; Rossi et al., 2018; Ruan et al., 2015; Zhai et al., 2008), and aging (Liu et al., 2018).

Humans have three nonredundant *Nmnat* genes, whereas *Drosophila melanogaster* has a single *Nmnat* gene (Ali et al., 2013) that is alternatively spliced into two distinct mRNA variants, RA and RB, giving rise to protein isoforms PC and PD, respectively (Ruan et al., 2015). Isoforms PC and PD share similar biochemical properties but have distinct subcellular localizations and divergent neuroprotective functions; isoform PD is cytosolic and a better neuroprotector than the RA-translated nuclear PC isoform (Ruan et al., 2015). A heat shock response element has been identified in the promoter of *Drosophila Nmnat*, allowing transcriptional upregulation of NMNAT pre-mRNA during stress conditions by stress transcription factor Heat Shock Factor (HSF) (Ali et al., 2011). Although NMNAT pre-mRNA is slightly preferentially spliced to RA during basal conditions, it has been shown that the splicing of NMNAT pre-mRNA is shifted to RB in response to stress. Even though NMNAT pre-mRNA transcription is upregulated, only NMNAT splice variant RB is increased in stress conditions. Thus, a post-transcriptional "switch" is activated to

[1]Department of Molecular and Cellular Pharmacology, University of Miami Miller School of Medicine, Miami, FL 33136, USA

[2]Program in Neuroscience, University of Miami Miller School of Medicine, Miami, FL 33136, USA

[3]Program in Molecular and Cellular Pharmacology, University of Miami Miller School of Medicine, Miami, FL 33136, USA

[4]Program in Human Genetics and Genomics, University of Miami Miller School of Medicine, Miami, FL 33136, USA

[5]Department of Computer Science, University of Miami, Coral Gables, FL 33146, USA

[6]Present address: Jennifer M. Brazill, Department of Medicine, Division of Bone and Mineral Diseases, Musculoskeletal Research Center, Washington University School of Medicine, St. Louis, MO 63110, USA

[7]Present address: Chong Li, Institute of Molecular Biotechnology of the Austrian Academy of Science (IMBA), Vienna 1030, Austria

[8]Lead Contact

*Correspondence: gzhai@med.miami.edu

https://doi.org/10.1016/j.isci.2019.08.052

 © 2019 The Author(s).
This is an open access article under the CC BY-NC-ND license (http://creativecommons.org/licenses/by-nc-nd/4.0/).

promote the splicing of NMNAT pre-mRNA to RB and to serve as an effective homeostasis strategy to increase the production of the more protective protein PD isoform under stress (Ruan et al., 2015). However, the identity of the "switch" and the mechanism of regulating NMNAT pre-mRNA alternative splicing under stress remain unknown.

MicroRNAs are short (~22 nt) noncoding RNAs involved in mRNA regulation (Carthew et al., 2017; Chawla et al., 2016). MicroRNAs typically bind complementary nucleotide sequences in the 3′ UTR of target mRNAs through the RNA-induced silencing complex (RISC) (O'Brien et al., 2018), which results in the degradation or translational repression of their targets (Gebert and MacRae, 2018). *Drosophila* Argonaute 1, the homolog of mammalian Argonaute 2, is the major RISC component onto which microRNAs are loaded (Yang et al., 2014). Although the vast majority of microRNA-target interactions result in decreased translation of the target, there are some reports of microRNAs upregulating translation of their target mRNAs (Cordes et al., 2009; Ghosh et al., 2008; Jopling et al., 2005; Lu et al., 2010; Mortensen et al., 2011; Ørom et al., 2008; Tsai et al., 2009; Vasudevan et al., 2007), often through binding the 5′UTR (Jopling et al., 2005; Ørom et al., 2008; Tsai et al., 2009). In addition, microRNAs have been implicated in stress response (Edeleva and Shcherbata, 2013; Matsuzaki and Ochiya, 2018; Münzel and Daiber, 2017; Wu et al., 2011) and homeostasis (Bijkerk et al., 2018; Çiçek et al., 2016). For example, miR-221 can protect human neurons from toxicity-induced stress (Oh et al., 2018), several microRNAs have been implicated in fine-tuning the redox stress response (Cheng et al., 2013), and miR-393a enhances stress tolerance (Zhao et al., 2018). We hypothesize that microRNAs mediate NMNAT splice variant expression under stress, owing to their ability to directly influence mRNA levels post-transcriptionally. We thus seek to identify potential microRNAs that are involved in the regulation of NMNAT-mediated stress resistance.

In this study, we identified *dme-miR-1002*, a microRNA with the ability to regulate alternative splicing by binding to NMNAT pre-mRNA and upregulating NMNAT mRNA variant RB. Furthermore, we found that *miR-1002* is critical to *Drosophila* thermotolerance and the stress response of NMNAT RB. Our findings suggest a previously unknown mode of gene expression regulation by non-coding RNAs and further reveal a new mechanism of maintaining homeostasis through stress resilience.

RESULTS

miR-1002 Knockout Flies Have Decreased NMNAT RB and PD Expression

Drosophila melanogaster has a single *Nmnat* gene producing two mRNA splice variants, RA and RB, which encode protein variants PC and PD, respectively. The pre-mRNA contains seven exons, with exons 1–4 commonly spliced and exons 5–7 alternatively spliced (Figure 1A). Since the enzymatic function required for NAD^+ synthesis is encoded in exons 1–4, both protein isoforms PC and PD have enzymatic activity (Ruan et al., 2015). Exon 7 encodes a nuclear localization motif; therefore, isoform PC including exons 6 and 7 is nuclear localized, whereas isoform PD including exon 5 is localized in the cytoplasm and confers robust neuroprotective function (Ruan et al., 2015).

To identify potential regulators of *Drosophila Nmnat* expression, we performed a putative microRNA seed sequence scan on NMNAT RB 3′UTR via microRNA.org (Enright et al., 2003; John et al., 2004) and identified *dme-miR-1002* among the highest scoring microRNAs (Figure 1A), with a miRSVR score of −0.5339, where miRSVR scores below −0.1 indicate high sensitivity and specificity (Betel et al., 2010).

To test if miR-1002 can modulate NMNAT RB levels, we obtained *miR-1002* homozygous knockout flies (*ΔmiR-1002*) and determined mRNA levels of variant RA and RB in heads by quantitative real-time PCR (Figure 1B). We observed significantly reduced levels of NMNAT RB, and increased RA, when compared with wild-type control (*yw*) flies. Furthermore, we found decreased NMNAT PD protein (Figures 1C and 1D) in the knockout flies. When we rescued these flies by conditional overexpression of miR-1002 in the knockout background (*ΔmiR-1002; elav-Geneswitch/UAS-miR-1002*), we observed a significant increase in NMNAT RB and a decrease in RA compared with knockout (Figure 1B). The rescue flies also had a significant increase in NMNAT PD (Figures 1C and 1D). This suggests that miR-1002 is important in regulating the expression of NMNAT RB mRNA and PD protein levels *in vivo*.

miR-1002 Shows No Effect in Altering the Stability of NMNAT RB

Reduced variant RB expression in *ΔmiR-1002* suggests that miR-1002 functions to increase the expression of its target mRNA, contrary to conventional 3′UTR-mediated mRNA degradation. To elucidate the

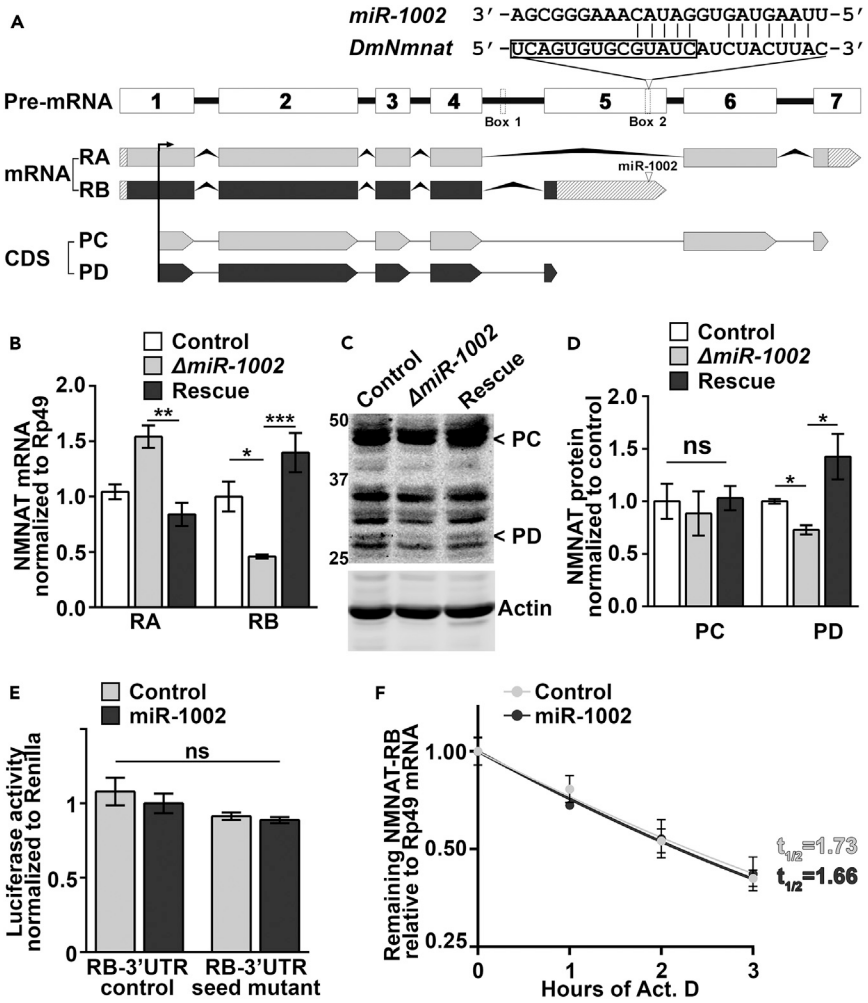

Figure 1. *miR-1002* Knockout Flies Have Decreased NMNAT RB and PD Expression

(A) Diagram showing *Drosophila* NMNAT pre-mRNA, mRNA splice variants, and protein isoforms. dme-miR-1002 binding sequence on *DmNmnat* depicted at top, with box around Box 2 sequences.

(B) NMNAT RNA levels in heads of control wild-type (*yw*), *miR-1002* homozygous knockout (*ΔmiR-1002*), and rescue flies (*ΔmiR-1002; UAS-miR-1002/elav-Geneswitch)*. Geneswitch flies were collected at 2DAE and fed RU486 for 5 days. RP49 used as reference gene. Normalized to control NMNAT RA. Bars indicate mean ± S.E.M. N = 4, One-Way ANOVA, Tukey's *post hoc*. *p < 0.05, **p < 0.01, ***p < 0.001.

(C) Western blot of control, *ΔmiR-1002,* and rescue fly heads. NMNAT PC and PD bands indicated at top. Actin loading control blot at bottom.

(D) Quantification of (C). Band intensities were normalized to actin, then control NMNAT levels set to 1. Bars indicate mean ± S.E.M. N = 4, ns, not significant; *p < 0.05, One-Way ANOVA, Tukey's *post hoc.*

(E) S2 cell dual luciferase activity assay. S2 cells were transfected with constructs expressing firefly luciferase linked to control wt NMNAT RB 3′UTR (RB 3′UTR control), firefly luciferase linked to NMNAT RB 3′UTR with the miR-1002 binding sequence mutated (RB 3′UTR seed mutant), or firefly luciferase only. In addition, miR-1002 or a scrambled miR-1002 control plasmid was transfected along with a Renilla luciferase plasmid. Firefly luciferase activity was normalized to Renilla luciferase activity levels, then standardized to the firefly luciferase only condition. Control + wt NMNAT RB 3′UTR was set to 1. Bars indicate mean ± S.E.M. N = 4, One-way ANOVA, Tukey's *post hoc.* ns, not significant.

(F) Actinomycin D chase assay. S2 cells were transfected with plasmids expressing miR-1002 or a scrambled miR-1002 control. RNA was collected at indicated time points after actinomycin D treatment, then NMNAT RB levels quantified by qPCR. Nonlinear regression was performed for NMNAT RB remaining (normalized to RP49) from initial amount at each time point. Points represent mean ± S.E.M. of N = 3 per condition per time point.

See also Figure S1.

molecular mechanisms of transcriptional regulation, we first tested the role of miR-1002 in 3′UTR-mediated mRNA stability using a dual luciferase activity assay (Figure 1E). Either the wild-type NMNAT RB 3′UTR sequence (RB 3′UTR control) or NMNAT RB 3′UTR with the miR-1002 seed sequence mutated (RB 3′UTR seed mutant) was inserted downstream of firefly luciferase in an expression vector. This plasmid was co-transfected into *Drosophila* S2 cells along with two additional plasmids: a Renilla luciferase expression plasmid (for transfection efficiency control) and either a plasmid overexpressing miR-1002 (miR-1002) or a control plasmid expressing a scrambled miR-1002 sequence (control). Forty-eight hours after transfection, we measured firefly and Renilla luciferase activity to test if miR-1002 can downregulate expression of firefly luciferase through NMNAT RB 3′UTR and if its binding sequence must be left intact for this to occur. In this reporter assay, we did not observe a significant difference in luciferase activity in cells co-transfected with the miR-1002 plasmid compared with the control plasmid. The same result was observed with both the wild-type and mutant NMNAT 3′UTR luciferase plasmids. This suggests that miR-1002 does not promote 3′UTR-mediated mRNA degradation.

However, it remains possible that miR-1002 can affect the stability of NMNAT RB indirectly through other regulatory pathways. To examine this possibility, we performed an actinomycin D chase assay where miR-1002 or a control was overexpressed by plasmid transfection in S2 cells and the endogenous NMNAT RB degradation rate was monitored after transcription was inhibited with actinomycin D (Qiu et al., 2016; Tew et al., 2014). As shown in Figure 1F, no significant difference in mRNA half-life for NMNAT RB was observed between cells expressing miR-1002 and control. Collectively, these results suggest that miR-1002 does not affect the stability of NMNAT RB in a 3′UTR-dependent or an indirect manner.

In Silico Analysis Reveals the miR-1002-Mediated Disruption of the Box 1-Box 2 Stem-Loop and Differential Minimum Free Energy Values in a Sequence-Specific Manner

To understand how *miR-1002* affects NMNAT expression, we examined its binding sequence relative to known regulatory elements. Two key elements in intron 4 and exon 5 have previously been found to be critical for alternative splicing (Raker et al., 2009). As shown in Figure 1A, complementary sequences in intron 4 (Box 1) and exon 5 (Box 2) must bind to form a pre-mRNA stem-loop to facilitate the skipping of exon 5 and inclusion of exon 6, thus forming the RA mRNA variant. When the stem-loop is not formed, exon 5 is preferentially spliced in, producing the RB variant.

The predicted binding sequence of miR-1002 overlaps Box 2 (Figure 1A, boxed nucleotides on DmNMNAT); we therefore hypothesized that miR-1002 binding to NMNAT pre-mRNA may interfere with formation of the stem-loop and shift splicing of NMNAT pre-mRNA toward RB. Furthermore, miR-1002 and NMNAT Box 2 sequences are conserved across *Drosophilae* (Figure S2). There is remarkable conservation of the Box 2 sequences on NMNAT which miR-1002 is predicted to bind (Figure S2A, red asterisks), and the sequence on miR-1002 that is predicted to bind them (Figure S2B, red asterisks). This highlights the evolutionary importance of these sequences in regulating NMNAT expression.

To test our hypothesis, we used an *in silico* approach to predict the RNA secondary structure of various NMNAT and miR-1002 duplexes. In particular, we determined the RNA secondary structure of wild-type exon 4 and intron 5 of NMNAT using RNAfold of the Vienna RNA package (Lorenz et al., 2011), utilizing default parameter settings. To visualize the corresponding minimum free energy structures, we utilized the FORNA web server (Kerpedjiev et al., 2015). We used this platform to model the structural consequences of miR-1002 binding to $NMNAT^{4-7}$, as well as the effects of various mutations on this interaction. As previously indicated (Raker et al., 2009), wild-type $NMNAT^{4-7}$ RNA sequence forms a stem-loop structure via complementary binding of Box 1 (cyan) and Box 2 (blue), a result that we corroborate with our folding of the secondary structure of wild-type NMNAT exon 4 and intron 5 (Figure 2A). Assuming that miR-1002 binds its predicted RNA sequence in Box 2, the ability of the corresponding nucleotides to bind other nucleotides in wild-type exon 4 and intron 5 of NMNAT is restricted. Simulating such an assumption, we constrained binding of the corresponding nucleotides using RNAfold, allowing us to observe a massive disruption of the stem-loop structure (Figure 2B). The $NMNAT^{4-7}$ mutations modeled in Figures 2C–2E encompass mutations within the miR-1002 binding sequence on NMNAT, precluding miR-1002 binding. When miR-1002's seed sequence outside of the binding stem is mutated (gray, mutated nucleotides in red), miR-1002 can no longer bind, allowing the stem-loop structure to form (Figure 2C). When miR-1002's binding sequence within Box 2 is mutated instead, miR-1002 binding is again impeded (Figure 2D). However, the stem-loop is expected to no longer form as a consequence of the disruption of

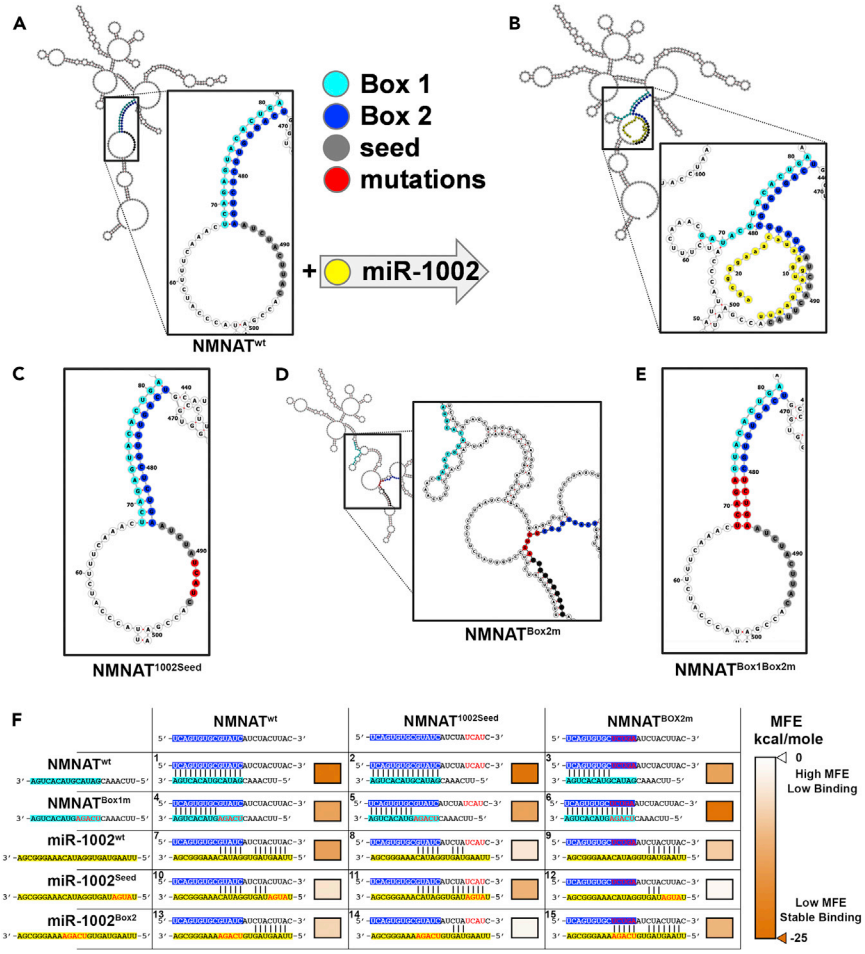

Figure 2. *In Silico* Analysis Reveals miR-1002-Mediated Disruption of Box 1-Box 2 Stem-Loop Secondary Structure and Differential MFE Values in a Sequence-Specific Manner

(A) FORNA minimum free energy model of the secondary structure of wt exon 4 and intron 5 sequences of NMNAT confirms the emergence of a stem between Box 1 (cyan) and Box 2 (blue) subsequences.

(B) miR-1002 (yellow) binds a putative seed sequence (gray) and sequences in Box 2, disrupting the stem.

(C–E) FORNA minimum free energy models of NMNAT where red sequences indicated nucleotide scrambled mutations.

(C) Scramble mutation to miR-1002 seed; (D) scramble mutation to Box 2; (E) Box 1/Box 2 scramble mutation.

(F) Minimum free energy values (kcal/mole) for various combinations of binding partners for NMNAT Box 2, calculated through duplexfold function in RNAStructure (Reuter and Mathews, 2010). Top row depicts the three NMNAT Box 2 variants used in this analysis-NMNAT^{wt}, the wild-type sequence of NMNAT Box 2 region; NMNAT^{1002Seed}, NMNAT Box 2 with 4 nucleotides in the miR-1002 seed sequence scrambled; NMNAT^{Box2m}, 5 nucleotides in Box 2 were scrambled. The left column depicts the five binding partners used—NMNAT^{wt}, the wild-type Box 1 region; NMNAT^{Box1m}, 5 nucleotides in Box 1 mutated in a complementary manner to the NMNAT^{Box2m} mutations; miR-1002^{wt}, the wild-type miR-1002-5p sequence; miR-1002^{Seed}, the seed sequence of miR-1002 mutated in a complementary manner to the NMNAT^{1002Seed} mutations; miR-1002^{Box2}, with the Box 2 sequences on miR-1002 mutated in a complementary manner to the NMNAT^{Box2m} mutations. Box to the right of each sequence depicts MFE of duplex binding based on color.

See also Figure S2.

the complementary sequences between Box 1 and Box 2. Finally, when sequences in Box 1 are mutated to be complementary to the Box 2 mutations, the stem-loop forms again (Figure 2E). However, corresponding mutations in the box 2 sequence prevent miR-1002 from binding.

We then probed the effects of various mutations to NMNAT and miR-1002 on the binding energy of the predicted duplex (Figure 2F). Using RNA Structure 6.1 (Reuter and Mathews, 2010), we calculated the minimum free energy of binding for various combinations of binding partners for NMNAT Box 2. The top row

depicts the NMNAT exon 5 sequence used in the modeling wild-type ($NMNAT^{wt}$), seed scramble ($NMNAT^{1002Seed}$, four nucleotides within miR-1002's seed sequence on NMNAT were scrambled to disrupt miR-1002 binding as in Figure 2C), and Box 2 scramble ($NMNAT^{Box2}$, five nucleotides within Box 2 were scrambled to disrupt miR-1002 binding as in Figure 2D). The left column shows the binding partners for NMNAT Box 2 used in this model. The top 2 are NMNAT Box 1 wild-type and NMNAT Box 1 scramble ($NMNAT^{Box1m}$, five nucleotides within Box 1 were scrambled in a complementary manner to the Box 2 scramble as in Figure 2E). The bottom three are wild-type miR-1002 (miR-1002^{wt}), seed scramble (miR-1002^{Seed}, four nucleotides within miR-1002's seed sequence scrambled in a complementary manner to $NMNAT^{1002seed}$, so as to restore miR-1002 binding), and Box 2 scramble (miR-1002^{Box2}, five nucleotides within miR-1002's Box 2 sequence scrambled in a complementary manner to $NMNAT^{Box2m}$, so as to restore miR-1002 binding).

Indeed, when miR-1002's binding to NMNAT is disrupted through mutations to the binding nucleotides ($NMNAT^{wt}$ + miR-1002^{Seed}(10), $NMNAT^{wt}$ + miR-1002^{Box2}(13), $NMNAT^{1002Seed}$ + miR-1002^{wt}(8), $NMNAT^{1002Seed}$ + miR-1002^{Box2}(14), $NMNAT^{Box2m}$ + miR-1002^{wt}(9), $NMNAT^{Box2m}$ + miR-1002^{wt}(12)), there is a significant increase in minimum free energy (MFE), indicating a less stable structure. MFE decreases when miR-1002 is mutated in a complementary manner to restore binding to NMNAT ($NMNAT^{1002Seed}$ + miR-1002^{Seed}(11), $NMNAT^{Box2m}$ + miR-1002^{Box2}(15)), indicating a strong and stable structure. In addition, Box 2 forming the stem-loop structure with Box 1 had low MFE values when the appropriate nucleotides were complementary ($NMNAT^{wt}$ + $NMNAT^{wt}$(1), $NMNAT^{1002Seed}$ + $NMNAT^{wt}$(2), $NMNAT^{Box2m}$ + $NMNAT^{Box1m}$(6)). Together, this analysis demonstrates how alternations in nucleotides have significant effects on the RNA secondary structure and binding energy and that the binding between miR-1002/Box 1 and Box 2 is direct and sequence specific.

miR-1002 Interferes with the Stem-Loop Mediated Alternative Splicing of NMNAT Pre-mRNA in a Sequence-Specific Manner

To experimentally verify our *in silico* modeling results, we developed a cellular reporter assay to test the functional consequences of various mutations on NMNAT splicing (Figure 3A). *Drosophila* S2 cells were transfected with a reporter plasmid containing firefly luciferase cDNA and NMNAT pre-mRNA exons 4–7 driven from a UAS promoter (pUAS-luc2-$NMNAT^{4-7}$). We co-transfected these cells with a plasmid expressing GAL4 and a scrambled miR-1002 sequence (pAC-GAL4-miR-1002-NegativeScramble) or wild-type miR-1002 (pAC-GAL4-miR-1002). The GAL4/UAS design ensures the co-expression of the Luc-$NMNAT^{4-7}$ reporter and miR-1002-GAL4. We then extracted RNA from these cells and determined NMNAT splice variant mRNA levels by qPCR. As shown in Figure 3B, overexpression of miR-1002 along with wild-type NMNAT reporter ($NMNAT^{wt}$) resulted in a significant increase in RB and decrease in RA (second set of bars) when compared with control (first set of bars). This is consistent with our hypothesis that miR-1002 interferes with stem-loop formation and shifts the splicing of NMNAT pre-mRNA toward NMNAT RB and away from RA. The upregulation of NMNAT RB by wild-type miR-1002 was not the result of increased transcription, as the RB/RA ratio was significantly increased (Figure S3A). When miR-1002 with its seed sequence mutated (third set of bars, corresponding to Figure 2F10) or its Box 2 sequence mutated (fourth set of bars, corresponding to Figure 2F13) was co-transfected along with the wild-type reporter, there was no effect on NMNAT splicing.

To determine the sequence specificity of miR-1002 in regulating NMNAT alternative splicing, we tested the mutations modeled in Figure 2. As shown in Figure 3C, when the miR-1002 seed sequence outside of NMNAT Box 2 was mutated such that wild-type miR-1002 could no longer bind as in Figure 2C ($NMNAT^{1002Seed}$), miR-1002 overexpression had no effect on RB expression (second set of bars, corresponding to Figure 2F8). This suggests that miR-1002 binding to its seed sequence is required for its effect on splicing. When miR-1002 itself was mutated in a complementary manner to restore binding, we observed a restoration of the downregulation in RA and upregulation in RB (far right bars, corresponding to Figure 2F11). Seed-mutated miR-1002 also increased the RB/RA ratio significantly (Figure S3B).

In contrast, when miR-1002's binding sequence within Box 2 was mutated to disrupt both stem-loop formation and miR-1002 binding as in Figure 2D ($NMNAT^{Box2m}$), there was no change in NMNAT variant expression in response to miR-1002 overexpression (Figure 3D). This was true with both wild-type miR-1002 (second set of bars) and miR-1002 with complementary mutations to NMNAT's Box 2 mutations to restore binding (third set of bars, corresponding to Figure 2F15). Additionally, the RB levels and RB/RA

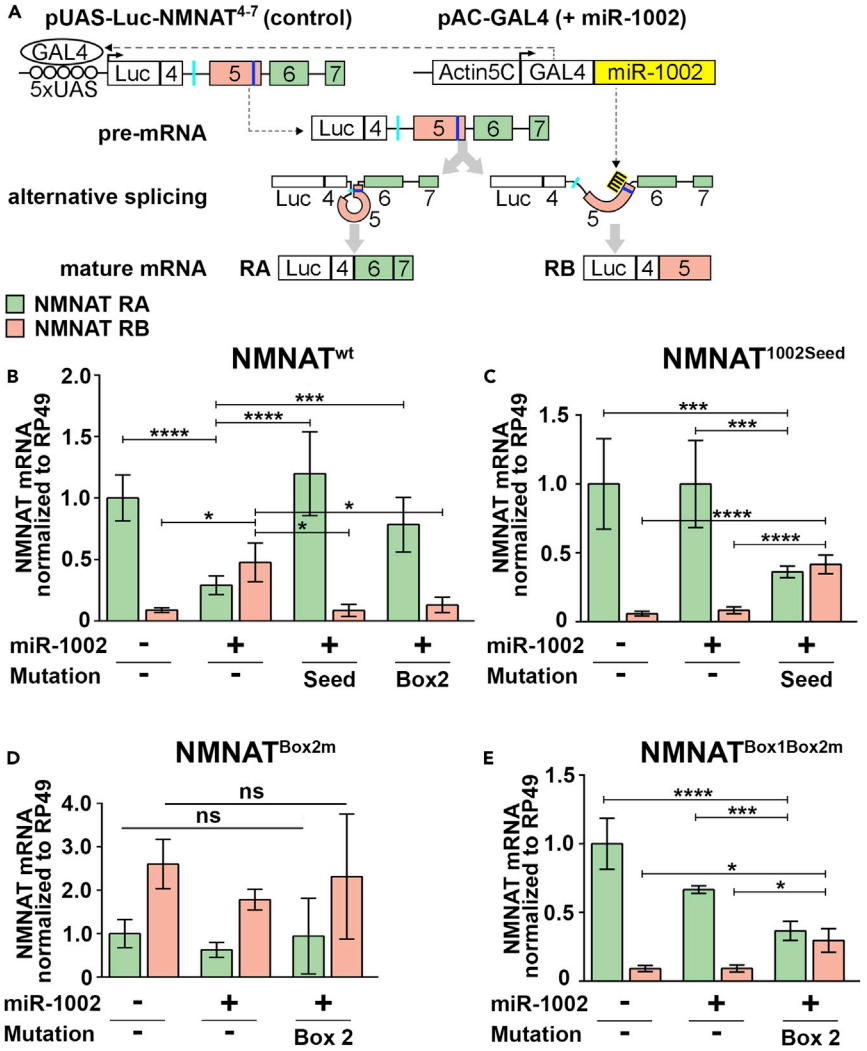

Figure 3. miR-1002 Interferes with the Stem-Loop Mediated Alternative Splicing of NMNAT Pre-mRNA in a Sequence-Specific Manner

(A) Schematic representation of S2 cell splicing assay. miR-1002 (yellow) is expressed from a pAC-GAL4 vector. GAL4 protein from pAC-GAL4 activates UAS elements in a reporter construct (pUAS-Luc2-NMNAT$^{4-7}$). Pre-mRNA from the reporter plasmid is then alternatively spliced into two variants. RNA is extracted from cells, then qPCR is performed for the mature NMNAT mRNA splice variants. This experiment was performed with combinations of the mutations introduced in Figure 2.

(B–E) Quantification of splicing assay. (B) wt pUASLuc-NMNAT$^{4-7}$ transfected with three different PAC-GAL4-miR-1002 variants (miR-1002^{wt}, second set of bars; miR-1002^{Seed}, third set of bars; miR-1002^{Box2}, fourth set of bars) and a negative control miR-1002 scramble plasmid (first set of bars). (C) pUAS-Luc2-NMNAT$^{4-7}$ Seed scramble (corresponding to NMNAT^{1002Seed} from Figure 2) transfected with two different PAC-GAL4-miR-1002 variants (miR-1002^{wt}, second set of bars; miR-1002^{seed}, third set of bars) and a negative control miR-1002 scramble plasmid (first set of bars). (D) pUAS-Luc2-NMNAT$^{4-7}$ Box2 scramble (corresponding to NMNAT^{Box2m} in Figure 2) transfected with two different PAC-GAL4-miR-1002 variants (miR-1002^{wt}, second set of bars; miR-1002^{Box2},third set of bars) and a negative control miR-1002 scramble plasmid (first set of bars). (E) pUAS-Luc2-NMNAT$^{4-7}$ Box1Box2 scramble (corresponding to NMNAT^{Box1Box2m} in Figure 2) transfected with two different PAC-GAL4-miR-1002 variants (miR-1002^{wt}, second set of bars; miR-1002^{Box2}, third set of bars) and a negative control miR-1002 scramble plasmid (first set of bars). Bars represent mean ± S.D. transcript levels for each condition and splice variant. Data were normalized to RP49 and control RA set to 1. N > 4, One-Way ANOVA, Tukey's *post hoc*, ns, not significant; *p < 0.05, ***p < 0.001. ****p < 0.0001.

See also Figure S3.

ratio (Figure S3C) for all conditions increased relative to the control wild-type Nmnat$^{4-7}$ plasmid, as the disruption of stem-loop results in exon 5 inclusion to produce RB. This further confirms the validity of our reporter system in assessing stem-loop formation.

Finally, when sequences in Box 1 were mutated in a complementary manner to the Box 2 mutations as in Figure 2E (NMNAT^{Box1Box2m}), RB levels decreased (Figure 3E) and the RB/RA ratio decreased (Figure S3D). This was expected since the complementary sequences of Box 1 and Box 2 allow the formation of the stem-loop and the exclusion of exon 5 to form RA. Although wild-type miR-1002 could not significantly alter NMNAT alternative splicing compared with control owing to its inability to bind NMNAT (first and second set of bars, corresponding to Figure 2F9), miR-1002 with a complementary Box 2 mutation was able to up-regulate RB and downregulate RA (third set of bars, corresponding to Figure 2F15). With miR-1002 able to bind to NMNAT again, it could compete with Box 1 for binding to Box 2 and increase the RB/RA splicing ratio (Figure S3D). Collectively, these results show that miR-1002 binding is necessary and sufficient to interfere with the stem-loop formation and shifts the splicing of NMNAT pre-mRNA to NMNAT RB.

miR-1002 Promotes the Inclusion of the RB-Exclusive Fifth Exon in an *In Vivo* Neuronal NMNAT Alternative Splicing Reporter

To assess if miR-1002 regulates the splicing of NMNAT pre-mRNA *in vivo*, we utilized a previously described alternative splicing reporter (Ruan et al., 2015), where the expression of AcGFP and DsRed are used as proxies for NMNAT RA and RB, respectively (Figure 4A). This is due to an in-frame AcGFP in the sixth exon and DsRed in the fifth exon.

Pan-neuronal overexpression of miR-1002 in the brain resulted in early lethality (data not shown). To overcome the lethality, we used an inducible Gene-switch (GS) driver (*elav-GS-GAL4*) to activate expression in adult flies. RU486 (Mifepristone) feeding for 5 days induced expression of the alternative splicing reporter (*UAS-NMNAT$^{4-7}$AltReport*) along with either miR-1002 (*UAS-miR-1002*), a non-targeting control microRNA miR-9a (*UAS-miR-9a*), or negative control luciferase (*UAS-Luc*). AcGFP and DsRed fluorescence in the fly brain was imaged and quantitated. As shown in Figure 4B, we observed a significantly higher DsRed and lower AcGFP fluorescence in the fly brain overexpressing miR-1002 when compared with controls (Figures 4C and 4D), indicating that miR-1002 overexpression promoted the inclusion of the fifth exon of the *NMNAT$^{4-7}$AltReport* splicing reporter construct. These results suggest that miR-1002 overexpression shifts the splicing of NMNAT pre-mRNA toward variant RB in neurons *in vivo*.

miR-1002 Mediates NMNAT Upregulation under Stress

NMNAT has been shown to protect many species against a variety of stresses, including heat, hypoxic, oxidative, proteotoxic, and aging stresses (Ali et al., 2012; Liu et al., 2018; Miwa et al., 2017; Rossi et al., 2018; Ruan et al., 2015; Zhou et al., 2016). Furthermore, it has previously been reported that *NMNAT* is a stress response gene regulated by the stress transcription factor HSF (Ali et al., 2011). Neuronal NMNAT PD protein and NMNAT RB mRNA, but not NMNAT RA, are upregulated in response to heat stress (Ruan et al., 2015). This demonstrates a stress-induced splicing "switch" to RB to confer increased protection. However, the mechanism of the variant-specific stress response "switch" to RB is unknown. miR-1002 presents an excellent candidate for this "switch" since it can bind to NMNAT pre-mRNA to obstruct the stem-loop formation and shift the splicing of NMNAT pre-mRNA into NMNAT RB. In addition, it has been reported that miR-1002 is upregulated in response to heat shock (Funikov et al., 2016) and oxidative stress induced by the treatment of a carcinogenic chemical Cr(VI) (Chandra et al., 2015). We wanted to investigate if the exclusive upregulation of NMNAT RB in these stress conditions is a result of miR-1002 enhancing the splicing of NMNAT pre-mRNA into RB. We subjected wild-type control *yw* and *ΔmiR-1002* flies to heat shock at 37°C for 45 min, a stress paradigm that has been shown to induce the highest level of NMNAT RB upregulation (Ruan et al., 2015). As expected, wild-type flies exhibited a significant upregulation in NMNAT RB but no significant change to RA in response to heat shock, whereas *ΔmiR-1002* flies lacked the increase in NMNAT RB in response to heat shock (Figure 5A). Moreover, there was a significant upregulation in NMNAT RA in the heat-shocked *ΔmiR-1002* flies. This supports a model in which NMNAT pre-mRNA transcription is increased during heat stress by heat shock transcription factor HSF, and the pre-mRNA is spliced almost exclusively to NMNAT RB owing to increased miR-1002. In the absence of miR-1002, the pre-mRNA is preferentially spliced into RA because of the structurally stable (low MFE) stem-loop formation.

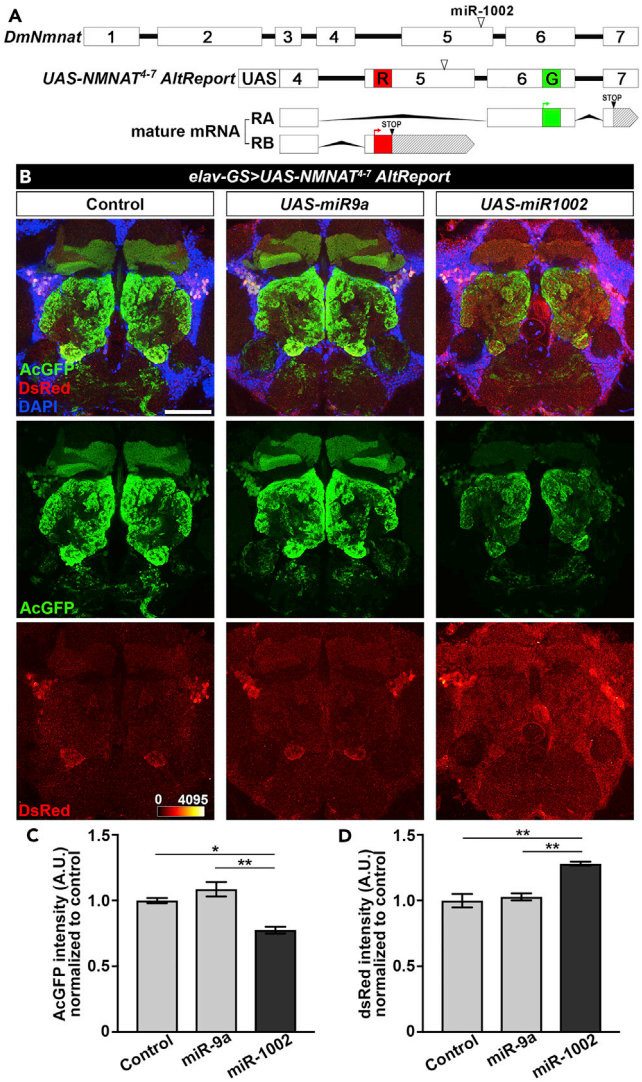

Figure 4. miR-1002 Promotes the Inclusion of the RB-exclusive Fifth Exon in an *In Vivo* Neuronal NMNAT Alternative Splicing Reporter Model

(A) Schematic representation of NMNAT reporter (*UAS-NMNAT$^{4-7}$ AltReport*) (Ruan et al., 2015). Genomic *NMNAT* at top with miR-1002 binding sequence indicated with white triangle. *NMNAT alternative splicing reporter* in middle, includes dsRed (Red R) in the fifth exon and AcGFP (Green G) in the sixth exon. Mature mRNA at bottom indicates RA-like splice variant with AcGFP, and RB-like variant with dsRed.

(B) Confocal images of fly brains expressing NMNAT reporter and miR-1002, control (Luciferase), or miR-9a. Scale bar, 50 μm.

(C and D) Quantification of (B). Bars represent mean of three midbrain areas per genotype ±S.E.M, normalized to control. N = 3, One-way ANOVA, Tukey's *post hoc*, *p < 0.05, **p < 0.01.

To assess the functional effects of *miR-1002* in stress response, we performed a thermotolerance assay whereby flies are subjected to a heat preconditioning (35°C for 30 min) followed by an extreme heat shock at 39°C, and the time to paralysis is recorded. It has been shown that loss of NMNAT leads to reduced latency to paralysis and that NMNAT overexpression confers paralysis resistance (Ali et al., 2011). As shown in Figure 5B, *ΔmiR-1002* flies had a reduced latency to paralysis compared with wild-type flies (p = 0.0031). The median survival time for control and *ΔmiR-1002* were 60 and 50 min, respectively. At 50 min, 54.086% of control flies remained active, compared with 41.154% of knockout flies. This suggests that miR-1002 is critical for thermotolerance and enhances stress resistance in part though upregulating NMNAT RB as one of the key targets in the stress response network.

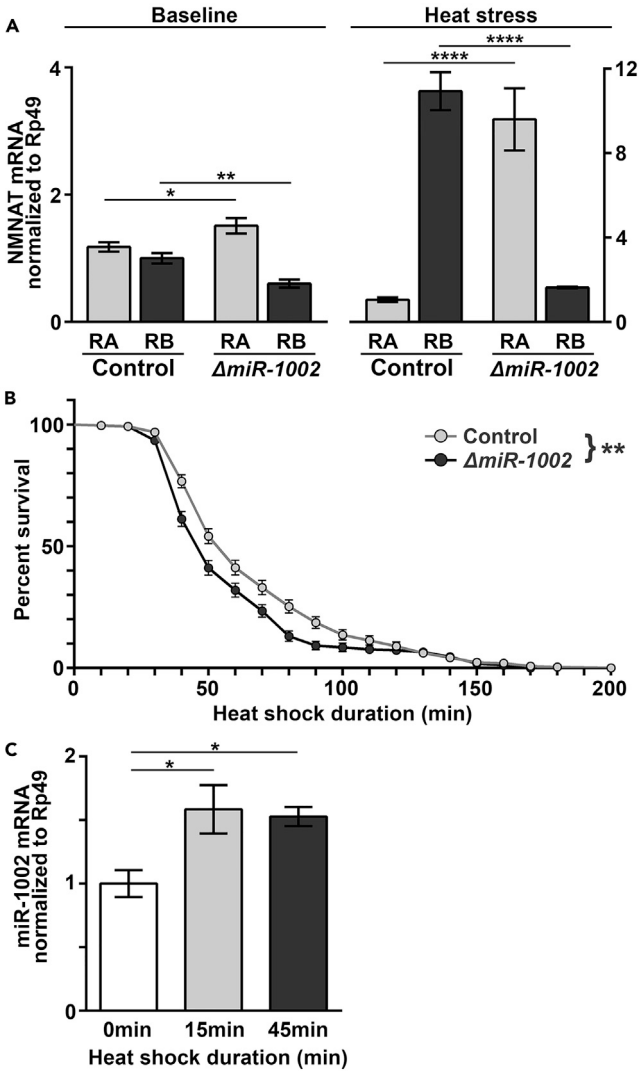

Figure 5. *miR-1002* Is Critical for Thermotolerance and the Upregulation of NMNAT RB under Heat Stress

(A) NMNAT RA and RB levels in control wild-type *yw* and *ΔmiR-1002* flies before and after heat shock. After NMNAT variant expression levels were normalized to RP49, control RB was set to 1. Bars represent mean ±S.E.M. N = 7 for baseline, N = 4 for heat stress. One-way ANOVA, Tukey's *post hoc*, *p < 0.05, **p < 0.01, ****p < 0.0001.

(B) Thermotolerance assay of control and *ΔmiR-1002* flies. Flies were subjected to heat shock and time taken to paralysis was recorded. Data points represent mean percent active flies at that time point. N > 200 flies, Log rank test. p = 0.0031.

(C) miR-1002 levels in heat shock. Wild-type flies were subjected to heat shock, and miR-1002 levels in heads quantified via qPCR and normalized to RP49 levels. Bars represent mean ±S.E.M. N=4, One-way ANOVA, Tukey's *post hoc*, *p < 0.05.

To determine if miR-1002 is upregulated during heat stress, we extracted the small RNA pool from wild-type fly heads after 15 and 45 min of heat shock. We detected a significant increase in miR-1002 level at both time points (Figure 5C). This demonstrates that miR-1002 is a heat-responsive microRNA and its increased transcription correlates with increased NMNAT splicing to RB. Higher levels of miR-1002 binding to NMNAT pre-mRNA facilitated efficient splicing to RB under stress.

Argonaute 1 Plays a Significant Role in miR-1002 Regulation of NMNAT Splicing

It has been well characterized that during RISC formation, mature *Drosophila* microRNAs are typically loaded onto Argonaute 1 before binding to target transcripts (Förstemann et al., 2007; Pushpavalli et al., 2012). We sought to determine the role of Argonaute 1 in miR-1002-mediated regulation of NMNAT splicing. We obtained Argonaute 1 hemizygous ($AGO1^{+/-}$) mutant flies, which had previously been shown

to have significantly reduced Argonaute 1 levels (Pushpavalli et al., 2014). Heat stress treatment of *AGO1*$^{+/-}$ flies resulted in no significant changes to RA or RB levels (Figure 6A), suggesting that Argonaute 1 is crucial to NMNAT's stress response.

The upregulation of NMNAT RB upon stress can be recapitulated by miR-1002 overexpression. A conditional overexpression of miR-1002 in fly brains resulted in a significant increase in NMNAT RB when compared with control LacZ overexpression (Figure 6B). In contrast, when miR-1002 was overexpressed in the *AGO1*$^{+/-}$ background, we observed an abrogation of the NMNAT RB upregulation. This substantiates the essential role of Argonaute 1 in miR-1002 regulation of splicing.

Since most splicing occurs co-transcriptionally in the nucleus (Carrillo Oesterreich et al., 2010), it is likely that AGO1-mediated miR-1002 regulation of splicing occurs in the nucleus. To investigate this possibility, we performed subcellular fractionation of S2 cells before and after heat shock to probe the nuclear, cytoplasmic, and whole-cell fractions for Argonaute 1, α-Tubulin (cytoplasmic marker), Calreticulin (ER marker [Gagnon et al., 2014]), and Histone H1 (nuclear marker) (Figures 6C and 6D). Argonaute 1 was present in the nuclear fraction (Figure 6C), and it was significantly increased in the nucleus after heat shock (Figure 6D). The lack of tubulin and calreticulin staining in the nuclear lanes indicates that there is no contamination from cytoplasmic or ER AGO1 in those fractions. To further validate this finding, we performed immunostaining on S2 cells before and after heat shock. As shown in Figures 6E and 6F, although the majority of Argonaute 1 protein was present in the cytoplasm under normal conditions, nuclear Argonaute 1 was significantly increased after heat shock. Additionally, we performed FISH for miR-1002 in S2 cells (Figure S4). We observed specific signal from the miR-1002 anti-sense probe in the nucleus of S2 cells, which suggests that miR-1002 can localize to the nucleus (Figure S4B). However, we did not observe significant change in miR-1002 FISH signals with heat shock. Thus, the stress-mediated localization of miR-1002 to the nucleus requires further analysis to confirm. Collectively, these results provide evidence for the potential role of Argonaute 1 in the stress-induced nuclear activity of miR-1002 and splicing of NMNAT.

DISCUSSION

In this study, we discovered a ground-breaking mechanism of a microRNA regulating gene expression under stress. Our results demonstrate that microRNA miR-1002 regulates NMNAT variant-specific expression by interfering with the fourth intron-fifth exon stem-loop formation required for pre-mRNA alternative splicing in a direct, sequence-specific manner, rather than by the canonical 3′UTR-mediated mRNA degradation. Additionally, we found that miR-1002 and RISC component Argonaute 1 are critical for NMNAT-mediated neuronal stress resistance.

A New Role for microRNAs in Transcriptional Regulation—MIMOSAS

This new mechanism of gene regulation, which we term MIMOSAS (MIcroRNA-Mediated Obstruction of Stem-loop Alternative Splicing) (Figure 7), presents a potential new layer through which cells can specifically control the expression of transcript variants. Although microRNAs are mostly studied in the context of mature mRNA 3′UTR binding and target transcript downregulation, MIMOSAS predicts the binding of microRNAs to interior intronic or exonic regions in the pre-mRNA of targets to regulate mRNA splicing. The outcome of such microRNA-pre-mRNA duplex binding allows mRNA expression modulation in an efficient and splice variant-specific manner. Importantly, MIMOSAS not only extends the functional repertoire of microRNAs, but also adds an exciting, novel example of long-range splicing and RNA secondary structure regulation (Gueroussov et al., 2017; Raker et al., 2009).

Previous studies have suggested that non-coding RNAs can affect splicing. Gonzalez, et al. showed that a long non-coding RNAs (lncRNA) can promote the retention of a particular exon in FGFR2 alternative splicing (Gonzalez et al., 2015). Double-stranded RNAs can affect the splicing of genes associated with muscular dystrophy (Liu et al., 2012). A small nuclear RNA has been found to regulate the splicing of Serotonin Receptor IIC, which is associated with Prader-Willi Syndrome (Kishore and Stamm, 2006).

miR-1002's ability to regulate splicing of a target transcript offers new insight to how microRNAs control gene expression. It remains to be seen how prevalent this mechanism is and whether it is conserved. It was previously reported that 42.6% of microRNA target sites in human T-REx 293 cells were found in mRNA CDS regions (Helwak et al., 2013). A study mapping Kaposi sarcoma-associated herpesvirus microRNA binding sites in B cell lymphoma-derived cells and epithelial cells found that a majority of microRNA

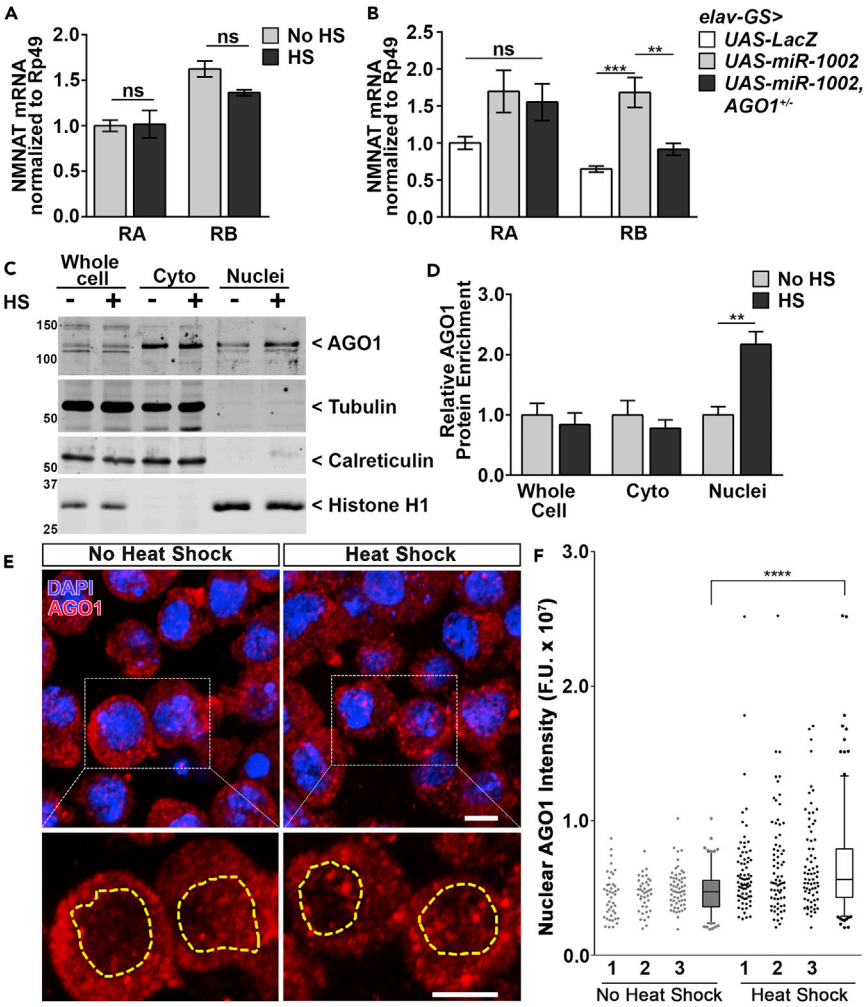

Figure 6. *Argonaute 1* Is Required for miR-1002-Mediated NMNAT Regulation

(A) NMNAT splice variant expression in response to heat shock in AGO1 hemizygous mutant flies. Flies were subjected to 45 min of heat shock at 37°C before RNA was extracted for qPCR. NMNAT levels normalized to RP49. No HS RA was set to 1. Bars represent as mean ± S.E.M. N = 4. One-way ANOVA, Tukey's *post hoc*.

(B) NMNAT splice variants in miR-1002 overexpression flies. Control flies expressing LacZ from an elav-geneswitch promoter, flies expressing miR-1002, and flies expressing miR-1002 in an AGO1 hemizygous mutant background were fed RU486 for 5 days, then RNA extracted from heads. NMNAT splice variant levels were normalized to RP49. Control RA was set to 1. Bars represent mean ±S.E.M. N=4, One-way ANOVA, Tukey's *post hoc*, ns, not significant; **$p < 0.01$, ***$p < 0.001$.

(C) Western blot of S2 cell fractions before and after heat shock. S2 cells were subjected to 1 h of heat shock at 37°C, then lysed to purify subcellular fractions. Total cell input, cytoplasm, and nuclei fractions were run together, then blotted for AGO1, Histone H1 (nuclear marker), Calreticulin (ER marker), and α-Tubulin (cytoplasmic marker).

(D) Quantification of (C). Band intensities of AGO1 were normalized to Tubulin for the total cell and cytoplasmic fractions, and Histone for the nucleic fractions. Approximately 6×10^4 cells loaded into each whole-cell lane, ~1×10^5 cells worth of cytoplasm in each cytoplasm lane, and ~3×10^5 nuclei loaded into the nuclei lanes. Each fraction was normalized to its no HS condition. Bars represent mean ±S.E.M. N = 4 One-way ANOVA, Tukey's *post hoc*, **$p < 0.01$.

(E) S2 cells were subjected to 1 h of heat shock at 37°C, then stained for DAPI and AGO1. Confocal microscopy was used to image and measure AGO1 in nuclei.

(F) Quantification of (E). 1–3 are 3 different experiments, with box plot for all experiments combined. Each dot represents a different cell. At least 140 cells were counted for each condition. Box represents upper quartile to lower quartile, with line to represent median. Whiskers represent 5 and 95 percentiles. Student's t test, ****$p < 0.0001$.

See also Figure S4.

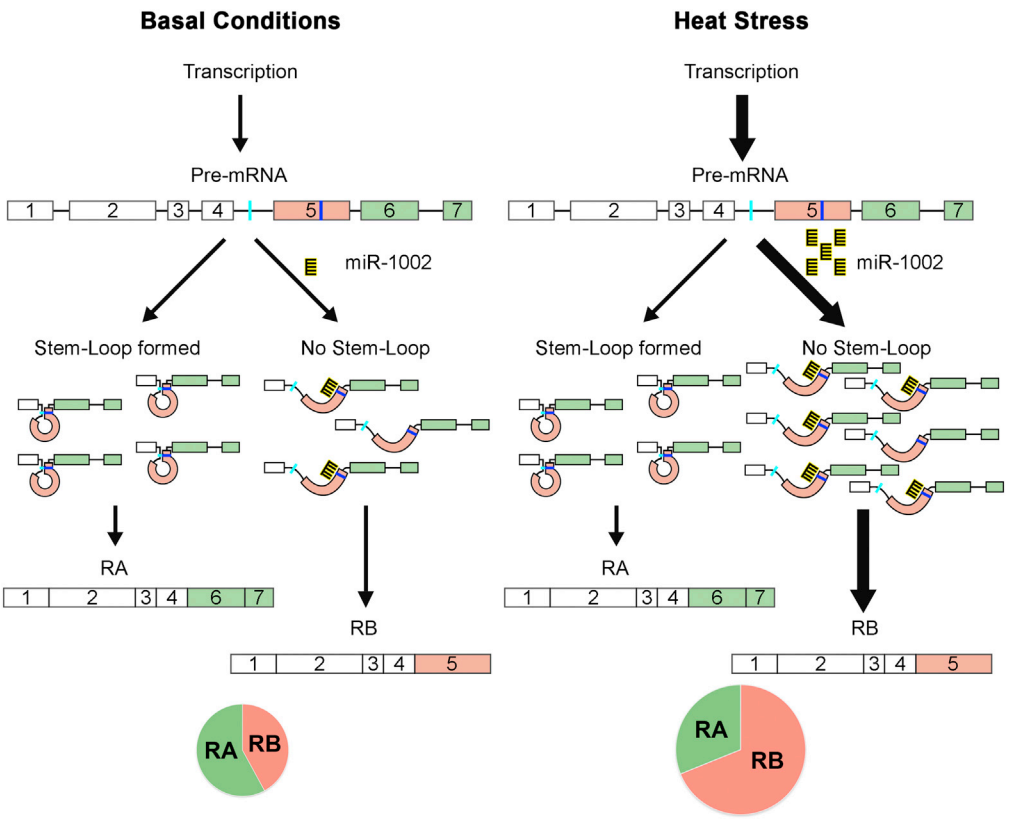

Figure 7. MIMOSAS, a Model for miR-1002 Regulation of NMNAT Splicing

Under basal conditions (left), NMNAT is preferentially spliced into the RA mRNA variant through stem-loop formation. Under stress (right), HSF upregulates transcription of NMNAT pre-mRNA. miR-1002 is also upregulated under stress, and miR-1002 enhances the splicing of NMNAT into the RB variant by preventing formation of the stem-loop. This upregulation serves as a stress-induced "switch" to increase protection through NMNAT PD.

target sites were found within the CDS of mRNAs, not the 3′UTR (Gay et al., 2018). Given that approximately 95% of multi-exonic human genes are alternatively spliced (Kim et al., 2018), microRNA target sites in the exonic and intronic regions present ample opportunities for microRNAs to target and influence pre-mRNA splicing.

Our findings suggest that MIMOSAS through miR-1002 is mediated by Argonaute 1. Since most splicing occurs co-transcriptionally (Oesterreich et al., 2016), the nucleus is the most likely location for such microRNA-mediated regulation. Supporting this hypothesis is the detection of microRNAs in the nucleus. RNALocate lists over 200 examples of experimentally determined nuclear non-coding RNAs in neuronal or neuron-like cells (Zhang et al., 2017). On the other hand, Argonautes have also been shown to be localized to the nucleus and bind chromatin (Cernilogar et al., 2011; Huang and Li, 2014; Huang et al., 2013; Pushpavalli et al., 2012; Taliaferro et al., 2013). For example, Argonaute has been found to be nuclear localized in many cell types, including T47D (Chu et al., 2010), 10G, ER293 (Ohrt et al., 2008), HEK293, HeLa, and RPE-1 cells (Rüdel et al., 2008). Our study detected Argonaute1 in the nuclear fraction, further supporting the notion that microRNA regulation of splicing may occur in the nuclear compartment. Specifically, our observation of the dependence of miR-1002 on Argonaute 1 and the stress-induced nuclear enrichment of Argonaute 1 supports a model in which Argonaute 1-miR-1002 localization to the nucleus during stress conditions facilitates the splicing of NMNAT pre-mRNA into the RB variant under stress.

MicroRNA miR-1002 Is a Part of the Stress Response Network

Our previous study has found that, under stress, the NMNAT RB variant is upregulated to produce the neuroprotective protein isoform (PD). Therefore, alternative splicing of NMNAT functions as a switch to

enhance neuroprotection under stress (Ruan et al., 2015). Excitingly, we discovered microRNA miR-1002 as the main driver of the "switch," as the upregulation of NMNAT RB under stress is eliminated in *ΔmiR-1002* flies (Figure 5A). Specifically, the observation that the heat shock upregulation of NMNAT RA in *ΔmiR-1002* flies mirrored the NMNAT RB increase in wild-type flies suggests that miR-1002 efficiently disrupts stem-loop and pushes all newly transcribed pre-mRNA into RB under stress. Without miR-1002, the newly transcribed NMNAT pre-mRNA was almost exclusively spliced to RA.

Our model predicts a novel role for miR-1002's regulation of NMNAT (Figure 7). In basal conditions, NMNAT pre-mRNA is spliced to RA with a slight preference via stem-loop formation (Ruan et al., 2015). Under stress, miR-1002 is upregulated and switches the splicing of newly transcribed NMNAT pre-mRNA almost exclusively to RB. Given the robust neuroprotective function of NMNAT isoform PD, miR-1002-mediated switch of alternative splicing enhances neuronal resistance to stress and confers organismal resilience. This is supported by the reduced thermotolerance observed in *ΔmiR-1002* flies. The modest reduction in thermotolerance suggests that miR-1002 is just one of the key players in the complex stress response network. Many other genes and proteins, including heat shock proteins, have been found to contribute to stress resistance (Bartelt-Kirbach et al., 2016; Jo et al., 2017; Kawasaki et al., 2016; Morrow et al., 2016; Shukla et al., 2014). Importantly, our study found that overexpression of miR-1002 in neurons was sufficient to shift alternative splicing toward RB *in vivo*, further substantiating the role of miR-1002 in enhancing NMNAT-mediated neuroprotection.

Our discovery of a novel mechanism of a microRNA regulating gene expression under stress unveils regulation of gene expression by noncoding RNAs in a state-specific manner and underscores the importance in considering alternative splicing modulation as therapeutic means. As 60% of point mutations associated with diseases have been found to be related to splicing defects (Jensen et al., 2009), several methods have been developed to modify alternative splicing. For example, duplex RNAs have also been used to modify alternative splicing in mammalian cells (Liu et al., 2012), and a method of using single-stranded siRNAs has been developed to modify the splicing of a Dystrophin RNA, which is associated with Duchenne muscular dystrophy (Liu et al., 2015). The results of our work introduce the possibility of microRNAs as tools to modulating alternative splicing. Although more work is required to identify other microRNA and target mRNA pairs, our work shows a promising new direction for conferring neuroprotection and organismal resilience.

Limitations of the Study

Although our data confirm the functional outcome, the mechanistic details of miR-1002 splicing regulation remain elusive. Furthermore, more work is needed to determine if this process is conserved in mammals and how prevalent the regulation of pre-mRNA splicing by microRNAs is.

METHODS

All methods can be found in the accompanying Transparent Methods supplemental file.

SUPPLEMENTAL INFORMATION

Supplemental Information can be found online at https://doi.org/10.1016/j.isci.2019.08.052.

ACKNOWLEDGMENTS

We would like to thank Zoraida Diaz-Perez and Kai Ruan for technical support. This research was supported by the National Institutes of Health (NIH) (R56NS095893 and R61AT010408 to R.G.Z.).

AUTHOR CONTRIBUTIONS

Conceptualization, J.P., S.W., and R.G.Z.; Methodology, J.P., X.T., S.W., and R.G.Z.; Investigation, J.P., X.T., Y.Z., J.M.B., C.L., and S.W.; Writing – Original Draft, J.P.; Writing – Review & Editing, J.P., Y.Z., C.L., J.M.B., S.W., and R.G.Z.; Visualization – J.P., Y.Z., J.M.B., C.L., and S.W; Funding Acquisition, R.G.Z.; Resources, S.W. and R.G.Z.; Supervision, R.G.Z.

DECLARATION OF INTERESTS

No conflicts of interest to declare.

Received: October 5, 2018
Revised: May 7, 2019
Accepted: August 27, 2019
Published: September 27, 2019

REFERENCES

Ali, Y.O., McCormack, R., Darr, A., and Zhai, R.G. (2011). Nicotinamide mononucleotide adenylyltransferase is a stress response protein regulated by the heat shock factor/hypoxia-inducible factor 1alpha pathway. J. Biol. Chem. *286*, 19089–19099.

Ali, Y.O., Ruan, K., and Zhai, R.G. (2012). NMNAT suppresses tau-induced neurodegeneration by promoting clearance of hyperphosphorylated tau oligomers in a Drosophila model of tauopathy. Hum. Mol. Genet. *21*, 237–250.

Ali, Y.O., Li-Kroeger, D., Bellen, H.J., Zhai, R.G., and Lu, H.-C. (2013). NMNATs, evolutionarily conserved neuronal maintenance factors. Trends Neurosci. *36*, 632–640.

Asatryan, A., and Bazan, N.G. (2017). Molecular mechanisms of signaling via the docosanoid neuroprotectin D1 for cellular homeostasis and neuroprotection. J. Biol. Chem. *292*, 12390–12397.

Bartelt-Kirbach, B., Moron, M., Glomb, M., Beck, C.-M., Weller, M.-P., and Golenhofen, N. (2016). HspB5/αB-crystallin increases dendritic complexity and protects the dendritic arbor during heat shock in cultured rat hippocampal neurons. Cell. Mol. Life Sci. *73*, 3761–3775.

Betel, D., Koppal, A., Agius, P., Sander, C., and Leslie, C. (2010). Comprehensive modeling of microRNA targets predicts functional non-conserved and non-canonical sites. Genome Biol. *11*, R90.

Bijkerk, R., Trimpert, C., van Solingen, C., de Bruin, R.G., Florijn, B.W., Kooijman, S., van den Berg, R., van der Veer, E.P., Bredewold, E.O.W., Rensen, P.C.N., et al. (2018). MicroRNA-132 controls water homeostasis through regulating MECP2-mediated vasopressin synthesis. Am. J. Physiol. Renal Physiol. *315*, F1129–F1138.

Brazill, J.M., Li, C., Zhu, Y., and Zhai, R.G. (2017). NMNAT: it's an NAD+ synthase… It's a chaperone… It's a neuroprotector. Curr. Opin. Genet. Dev. *44*, 156–162.

Carrillo Oesterreich, F., Preibisch, S., and Neugebauer, K.M. (2010). Global analysis of nascent RNA reveals transcriptional pausing in terminal exons. Mol. Cell *40*, 571–581.

Carthew, R.W., Agbu, P., and Giri, R. (2017). MicroRNA function in *Drosophila melanogaster*. Semin. Cell Dev. Biol. *65*, 29–37.

Cernilogar, F.M., Onorati, M.C., Kothe, G.O., Burroughs, A.M., Parsi, K.M., Breiling, A., Lo Sardo, F., Saxena, A., Miyoshi, K., Siomi, H., et al. (2011). Chromatin-associated RNAi components contribute to transcriptional regulation in Drosophila. Nature *480*, 391–395.

Chandra, G., Shenoi, R.A., Anand, R., Rajamma, U., and Mohanakumar, K.P. (2017). Reinforcing mitochondrial functions in aging brain: an insight into Parkinson's disease therapeutics. J. Chem. Neuroanat. *95*, 29–42.

Chandra, S., Pandey, A., and Chowdhuri, D.K. (2015). MiRNA profiling provides insights on adverse effects of Cr(VI) in the midgut tissues of *Drosophila melanogaster*. J. Hazard. Mater. *283*, 558–567.

Chandran, R., Kumar, M., Kesavan, L., Jacob, R.S., Gunasekaran, S., Lakshmi, S., Sadasivan, C., and Omkumar, R.V. (2017). Cellular calcium signaling in the aging brain. J. Chem. Neuroanat. *95*, 95–114.

Chawla, G., Luhur, A., and Sokol, N. (2016). Analysis of MicroRNA function in Drosophila. Methods Mol. Biol. *1478*, 79–94.

Cheng, X., Ku, C.-H., and Siow, R.C.M. (2013). Regulation of the Nrf2 antioxidant pathway by microRNAs: new players in micromanaging redox homeostasis. Free Radic. Biol. Med. *64*, 4–11.

Chiurchiù, V., Orlacchio, A., and Maccarrone, M. (2016). Is modulation of oxidative stress an answer? the state of the art of redox therapeutic actions in neurodegenerative diseases. Oxid. Med. Cell. Longev. *2016*, 7909380.

Chu, Y., Yue, X., Younger, S.T., Janowski, B.A., and Corey, D.R. (2010). Involvement of argonaute proteins in gene silencing and activation by RNAs complementary to a non-coding transcript at the progesterone receptor promoter. Nucleic Acids Res. *38*, 7736–7748.

Çiçek, I.Ö., Karaca, S., Brankatschk, M., Eaton, S., Urlaub, H., and Shcherbata, H.R. (2016). Hedgehog signaling strength is orchestrated by the mir-310 cluster of MicroRNAs in response to diet. Genetics *202*, 1167–1183.

Cobley, J.N., Fiorello, M.L., and Bailey, D.M. (2018). 13 reasons why the brain is susceptible to oxidative stress. Redox Biol. *15*, 490–503.

Cordes, K.R., Sheehy, N.T., White, M.P., Berry, E.C., Morton, S.U., Muth, A.N., Lee, T.-H., Miano, J.M., Ivey, K.N., and Srivastava, D. (2009). miR-145 and miR-143 regulate smooth muscle cell fate and plasticity. Nature *460*, 705–710.

Edeleva, E.V., and Shcherbata, H.R. (2013). Stress-induced ECM alteration modulates cellular microRNAs that feedback to readjust the extracellular environment and cell behavior. Front. Genet. *4*, 305.

Enright, A.J., John, B., Gaul, U., Tuschl, T., Sander, C., and Marks, D.S. (2003). MicroRNA targets in Drosophila. Genome Biol. *5*, R1.

Fang, Y., Soares, L., Teng, X., Geary, M., and Bonini, N.M. (2012). A novel Drosophila model of nerve injury reveals an essential role of Nmnat in maintaining axonal integrity. Curr. Biol. *22*, 590–595.

Förstemann, K., Horwich, M.D., Wee, L., Tomari, Y., and Zamore, P.D. (2007). Drosophila microRNAs are sorted into functionally distinct Argonaute protein complexes after their production by Dicer-1. Cell *130*, 287–297.

Funikov, S.Y., Ryazansky, S.S., Kanapin, A.A., Logacheva, M.D., Penin, A.A., Snezhkina, A.V., Shilova, V.Y., Garbuz, D.G., Evgen'ev, M.B., and Zatsepina, O.G. (2016). Interplay between RNA interference and heat shock response systems in *Drosophila melanogaster*. Open Biol. *6*, https://doi.org/10.1098/rsob.160224.

Gagnon, K.T., Li, L., Chu, Y., Janowski, B.A., and Corey, D.R. (2014). RNAi factors are present and active in human cell nuclei. Cell Rep. *6*, 211–221.

Gay, L.A., Sethuraman, S., Thomas, M., Turner, P.C., and Renne, R. (2018). Modified cross-linking, ligation, and sequencing of hybrids (qCLASH) identifies Kaposi's sarcoma-associated herpesvirus microrna targets in endothelial cells. J. Virol. *92*, e02138–17.

Gebert, L.F.R., and MacRae, I.J. (2018). Regulation of microRNA function in animals. Nat. Rev. Mol. Cell Biol. *20*, 21–37.

Ghosh, T., Soni, K., Scaria, V., Halimani, M., Bhattacharjee, C., and Pillai, B. (2008). MicroRNA-mediated up-regulation of an alternatively polyadenylated variant of the mouse cytoplasmic {beta}-actin gene. Nucleic Acids Res. *36*, 6318–6332.

Gonzalez, I., Munita, R., Agirre, E., Dittmer, T.A., Gysling, K., Misteli, T., and Luco, R.F. (2015). A lncRNA regulates alternative splicing via establishment of a splicing-specific chromatin signature. Nat. Struct. Mol. Biol. *22*, 370–376.

Gueroussov, S., Weatheritt, R.J., O'Hanlon, D., Lin, Z.-Y., Narula, A., Gingras, A.-C., and Blencowe, B.J. (2017). Regulatory expansion in mammals of multivalent hnRNP assemblies that globally control alternative splicing. Cell *170*, 324–339.e23.

Helwak, A., Kudla, G., Dudnakova, T., and Tollervey, D. (2013). Mapping the human miRNA interactome by CLASH reveals frequent noncanonical binding. Cell *153*, 654–665.

Huang, V., and Li, L.-C. (2014). Demystifying the nuclear function of Argonaute proteins. RNA Biol. *11*, 18–24.

Huang, V., Zheng, J., Qi, Z., Wang, J., Place, R.F., Yu, J., Li, H., and Li, L.-C. (2013). Ago1 Interacts with RNA polymerase II and binds to the promoters of actively transcribed genes in human cancer cells. PLoS Genet. *9*, e1003821.

Jensen, C.J., Oldfield, B.J., and Rubio, J.P. (2009). Splicing, cis genetic variation and disease. Biochem. Soc. Trans. *37*, 1311–1315.

Jo, H.S., Kim, D.W., Shin, M.J., Cho, S.B., Park, J.H., Lee, C.H., Yeo, E.J., Choi, Y.J., Yeo, H.J., Sohn, E.J., et al. (2017). Tat-HSP22 inhibits oxidative stress-induced hippocampal neuronal cell death by regulation of the mitochondrial pathway. Mol. Brain *10*, 1.

John, B., Enright, A.J., Aravin, A., Tuschl, T., Sander, C., and Marks, D.S. (2004). Human MicroRNA targets. PLoS Biol. *2*, e363.

Jopling, C.L., Yi, M., Lancaster, A.M., Lemon, S.M., and Sarnow, P. (2005). Modulation of hepatitis C virus RNA abundance by a liver-specific MicroRNA. Science *309*, 1577–1581.

Kagias, K., Nehammer, C., and Pocock, R. (2012). Neuronal responses to physiological stress. Front. Genet. *3*, 222.

Kawasaki, F., Koonce, N.L., Guo, L., Fatima, S., Qiu, C., Moon, M.T., Zheng, Y., and Ordway, R.W. (2016). Small heat shock proteins mediate cell-autonomous and -nonautonomous protection in a Drosophila model for environmental-stress-induced degeneration. Dis. Model. Mech. *9*, 953–964.

Kerpedjiev, P., Hammer, S., and Hofacker, I.L. (2015). Forna (force-directed RNA): simple and effective online RNA secondary structure diagrams. Bioinformatics *31*, 3377–3379.

Kim, K.W., and Jin, Y. (2015). Neuronal responses to stress and injury in C. elegans. FEBS Lett. *589*, 1644–1652.

Kim, H.K., Pham, M.H.C., Ko, K.S., Rhee, B.D., and Han, J. (2018). Alternative splicing isoforms in health and disease. Pflugers Arch. *470*, 995–1016.

Kirkwood, T.B.L. (2003). The most pressing problem of our age. BMJ *326*, 1297–1299.

Kishore, S., and Stamm, S. (2006). The snoRNA HBII-52 regulates alternative splicing of the serotonin receptor 2C. Science *311*, 230–232.

Kitaoka, Y., Munemasa, Y., Kojima, K., Hirano, A., Ueno, S., and Takagi, H. (2013). Axonal protection by Nmnat3 overexpression with involvement of autophagy in optic nerve degeneration. Cell Death Dis. *4*, e860.

Liu, J., Hu, J., and Corey, D.R. (2012). Expanding the action of duplex RNAs into the nucleus: redirecting alternative splicing. Nucleic Acids Res. *40*, 1240–1250.

Liu, J., Hu, J., Hicks, J.A., Prakash, T.P., and Corey, D.R. (2015). Modulation of splicing by single-stranded silencing RNAs. Nucleic Acid Ther. *25*, 113–120.

Liu, X., Xiang, Z., Li, Q., Ruan, X., Xiong, K., Dengtai, W., and Zheng, L. (2018). Overexpression of Nmnat improves the adaption of health span in aging Drosophila. Exp. Gerontol. *108*, 276–283.

Lorenz, R., Bernhart, S.H., Höner Zu Siederdissen, C., Tafer, H., Flamm, C., Stadler, P.F., and Hofacker, I.L. (2011). ViennaRNA package 2.0. Algorithms Mol. Biol. *6*, 26.

Lu, H., Buchan, R.J., and Cook, S.A. (2010). MicroRNA-223 regulates Glut4 expression and cardiomyocyte glucose metabolism. Cardiovasc. Res. *86*, 410–420.

Matsuzaki, J., and Ochiya, T. (2018). Extracellular microRNAs and oxidative stress in liver injury: a systematic mini review. J. Clin. Biochem. Nutr. *63*, 6–11.

Miwa, A., Sawada, Y., Tamaoki, D., Yokota Hirai, M., Kimura, M., Sato, K., and Nishiuchi, T. (2017). Nicotinamide mononucleotide and related metabolites induce disease resistance against fungal phytopathogens in Arabidopsis and barley. Sci. Rep. *7*, 6389.

Morrow, G., Le Pécheur, M., and Tanguay, R.M. (2016). Drosophila melanogaster mitochondrial Hsp22: a role in resistance to oxidative stress, aging and the mitochondrial unfolding protein response. Biogerontology *17*, 61–70.

Mortensen, R.D., Serra, M., Steitz, J.A., and Vasudevan, S. (2011). Posttranscriptional activation of gene expression in *Xenopus laevis* oocytes by microRNA-protein complexes (microRNPs). Proc. Natl. Acad. Sci. U S A *108*, 8281–8286.

Münzel, T., and Daiber, A. (2017). Environmental stressors and their impact on health and disease with focus on oxidative stress. Antioxid. Redox Signal. *28*, 735–740.

O'Brien, J., Hayder, H., Zayed, Y., and Peng, C. (2018). Overview of microRNA biogenesis, mechanisms of actions, and circulation. Front. Endocrinol. (Lausanne) *9*, 402.

Oesterreich, F.C., Herzel, L., Straube, K., Hujer, K., Howard, J., and Neugebauer, K.M. (2016). Splicing of nascent RNA coincides with intron exit from RNA polymerase II. Cell *165*, 372–381.

Oh, S.E., Park, H.-J., He, L., Skibiel, C., Junn, E., and Mouradian, M.M. (2018). The Parkinson's disease gene product DJ-1 modulates miR-221 to promote neuronal survival against oxidative stress. Redox Biol. *19*, 62–73.

Ohrt, T., Mütze, J., Staroske, W., Weinmann, L., Höck, J., Crell, K., Meister, G., and Schwille, P. (2008). Fluorescence correlation spectroscopy and fluorescence cross-correlation spectroscopy reveal the cytoplasmic origination of loaded nuclear RISC in vivo in human cells. Nucleic Acids Res. *36*, 6439–6449.

Ørom, U.A., Nielsen, F.C., and Lund, A.H. (2008). MicroRNA-10a binds the 5'UTR of ribosomal protein mRNAs and enhances their translation. Mol. Cell *30*, 460–471.

Orsini, M., Nascimento, O.J.M., Matta, A.P.C., Reis, C.H.M., de Souza, O.G., Bastos, V.H., Moreira, R., Ribeiro, P., Fiorelli, S., Novellino, P., et al. (2016). Revisiting the term neuroprotection in chronic and degenerative diseases. Neurol. Int. *8*, 6311.

Press, C., and Milbrandt, J. (2008). Nmnat delays axonal degeneration caused by mitochondrial and oxidative stress. J. Neurosci. *28*, 4861–4871.

Pushpavalli, S.N.C.V.L., Bag, I., Pal-Bhadra, M., and Bhadra, U. (2012). Drosophila Argonaute-1 is critical for transcriptional cosuppression and heterochromatin formation. Chromosome Res. *20*, 333–351.

Pushpavalli, S.N.C.V.L., Sarkar, A., Bag, I., Hunt, C.R., Ramaiah, M.J., Pandita, T.K., Bhadra, U., and Pal-Bhadra, M. (2014). Argonaute-1 functions as a mitotic regulator by controlling Cyclin B during Drosophila early embryogenesis. FASEB J. *28*, 655–666.

Qiu, L.-Q., Lai, W.S., Stumpo, D.J., and Blackshear, P.J. (2016). Measurement of mRNA decay in mouse embryonic fibroblasts. Bio Protoc. *6*, https://doi.org/10.21769/BioProtoc.1858.

Raker, V.A., Mironov, A.A., Gelfand, M.S., and Pervouchine, D.D. (2009). Modulation of alternative splicing by long-range RNA structures in Drosophila. Nucleic Acids Res. *37*, 4533–4544.

Reuter, J.S., and Mathews, D.H. (2010). RNAstructure: software for RNA secondary structure prediction and analysis. BMC Bioinformatics *11*, 129.

Rossi, F., Geiszler, P.C., Meng, W., Barron, M.R., Prior, M., Herd-Smith, A., Loreto, A., Lopez, M.Y., Faas, H., Pardon, M.-C., et al. (2018). NAD-biosynthetic enzyme NMNAT1 reduces early behavioral impairment in the htau mouse model of tauopathy. Behav. Brain Res. *339*, 140–152.

Ruan, K., Zhu, Y., Li, C., Brazill, J.M., and Zhai, R.G. (2015). Alternative splicing of Drosophila Nmnat functions as a switch to enhance neuroprotection under stress. Nat. Commun. *6*, 10057.

Rüdel, S., Flatley, A., Weinmann, L., Kremmer, E., and Meister, G. (2008). A multifunctional human Argonaute2-specific monoclonal antibody. RNA *14*, 1244–1253.

Sasaki, Y., and Milbrandt, J. (2010). Axonal degeneration is blocked by nicotinamide mononucleotide adenylyltransferase (Nmnat) protein transduction into transected axons. J. Biol. Chem. *285*, 41211–41215.

Sasaki, Y., Vohra, B.P.S., Baloh, R.H., and Milbrandt, J. (2009). Transgenic mice expressing the Nmnat1 protein manifest robust delay in axonal degeneration in vivo. J. Neurosci. *29*, 6526–6534.

Saxena, S., and Caroni, P. (2011). Selective neuronal vulnerability in neurodegenerative diseases: from stressor thresholds to degeneration. Neuron *71*, 35–48.

Shukla, A.K., Pragya, P., Chaouhan, H.S., Tiwari, A.K., Patel, D.K., Abdin, M.Z., and Chowdhuri, D.K. (2014). Heat shock protein-70 (Hsp-70) suppresses paraquat-induced neurodegeneration by inhibiting JNK and caspase-3 activation in Drosophila model of Parkinson's disease. PLoS One *9*, e98886.

Taliaferro, J.M., Aspden, J.L., Bradley, T., Marwha, D., Blanchette, M., and Rio, D.C. (2013). Two new and distinct roles for Drosophila Argonaute-2 in the nucleus: alternative pre-mRNA splicing and transcriptional repression. Genes Dev. *27*, 378–389.

Tew, S.R., McDermott, B.T., Fentem, R.B., Peffers, M.J., and Clegg, P.D. (2014). Transcriptome-wide analysis of messenger RNA decay in normal and osteoarthritic human articular chondrocytes. Arthritis Rheumatol. *66*, 3052–3061.

Tsai, N.-P., Lin, Y.-L., and Wei, L.-N. (2009). MicroRNA mir-346 targets the 5'-untranslated

region of receptor-interacting protein 140 (RIP140) mRNA and up-regulates its protein expression. Biochem. J. *424*, 411–418.

Vasudevan, S., Tong, Y., and Steitz, J.A. (2007). Switching from repression to activation: microRNAs can up-regulate translation. Science *318*, 1931–1934.

Wen, Y., Parrish, J.Z., He, R., Zhai, R.G., and Kim, M.D. (2011). Nmnat exerts neuroprotective effects in dendrites and axons. Mol. Cell. Neurosci. *48*, 1–8.

Wen, Y., Zhai, R.G., and Kim, M.D. (2013). The role of autophagy in Nmnat-mediated protection against hypoxia-induced dendrite degeneration. Mol. Cell. Neurosci. *52*, 140–151.

Wu, C., So, J., Davis-Dusenbery, B.N., Qi, H.H., Bloch, D.B., Shi, Y., Lagna, G., and Hata, A. (2011). Hypoxia potentiates MicroRNA-mediated gene silencing through posttranslational modification of Argonaute2. Mol. Cell. Biol. *31*, 4760–4774.

Yan, T., Feng, Y., Zheng, J., Ge, X., Zhang, Y., Wu, D., Zhao, J., and Zhai, Q. (2010). Nmnat2 delays axon degeneration in superior cervical ganglia dependent on its NAD synthesis activity. Neurochem. Int. *56*, 101–106.

Yang, J.-S., Smibert, P., Westholm, J.O., Jee, D., Maurin, T., and Lai, E.C. (2014). Intertwined pathways for Argonaute-mediated microRNA biogenesis in Drosophila. Nucleic Acids Res. *42*, 1987–2002.

Zhai, R.G., Cao, Y., Hiesinger, P.R., Zhou, Y., Mehta, S.Q., Schulze, K.L., Verstreken, P., and Bellen, H.J. (2006). Drosophila NMNAT maintains neural integrity independent of its NAD synthesis activity. PLoS Biol. *4*, e416.

Zhai, R.G., Zhang, F., Hiesinger, P.R., Cao, Y., Haueter, C.M., and Bellen, H.J. (2008). NAD synthase NMNAT acts as a chaperone to protect against neurodegeneration. Nature *452*, 887–891.

Zhai, R.G., Rizzi, M., and Garavaglia, S. (2009). Nicotinamide/nicotinic acid mononucleotide adenylyltransferase, new insights into an ancient enzyme. Cell. Mol. Life Sci. *66*, 2805–2818.

Zhang, T., Tan, P., Wang, L., Jin, N., Li, Y., Zhang, L., Yang, H., Hu, Z., Zhang, L., Hu, C., et al. (2017). RNALocate: a resource for RNA subcellular localizations. Nucleic Acids Res. *45*, D135–D138.

Zhao, J., Yuan, S., Zhou, M., Yuan, N., Li, Z., Hu, Q., Bethea, F.G., Liu, H., Li, S., and Luo, H. (2018). Transgenic creeping bentgrass overexpressing Osa-miR393a exhibits altered plant development and improved multiple stress tolerance. Plant Biotechnol. J. *17*, 233–251.

Zhou, R.-M., Shen, Y., Yao, J., Yang, H., Shan, K., Li, X.-M., Jiang, Q., and Yan, B. (2016). Nmnat 1: a security guard of retinal ganglion cells (RGCs) in response to high glucose stress. Cell. Physiol. Biochem. *38*, 2207–2218.

ISCI, Volume *19*

Supplemental Information

MicroRNA miR-1002 Enhances NMNAT-Mediated Stress Response by Modulating Alternative Splicing

Joun Park, Yi Zhu, Xianzun Tao, Jennifer M. Brazill, Chong Li, Stefan Wuchty, and R. Grace Zhai

Supplemental Information

Supplemental Figures

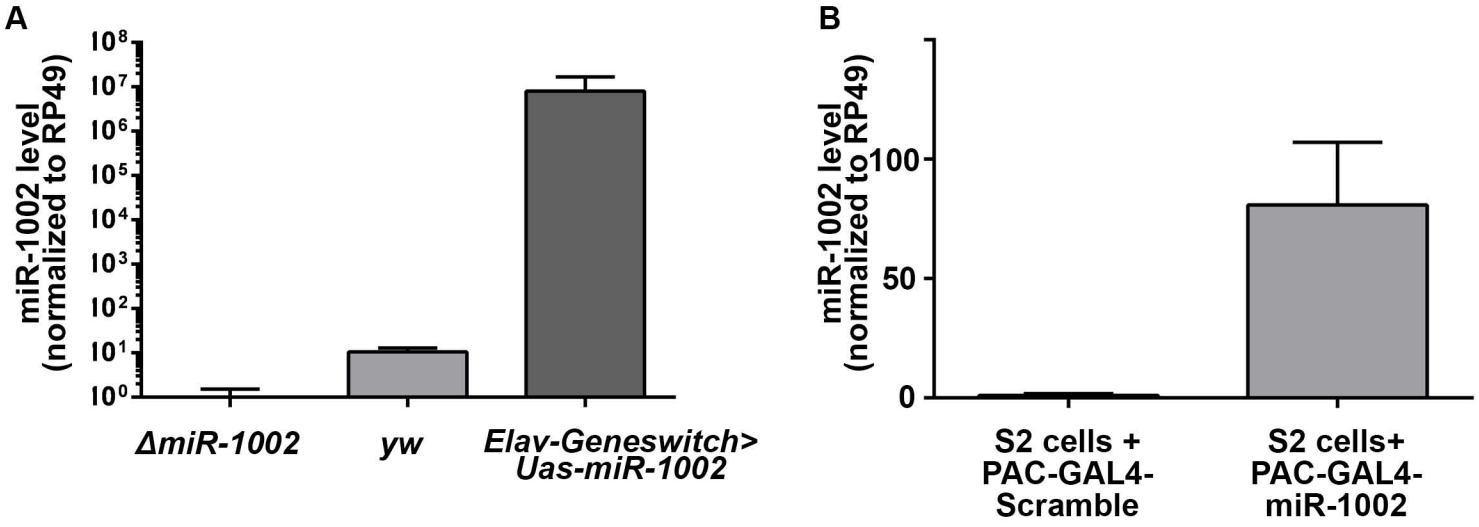

Figure S1. miR-1002 overexpression is robust in both flies and S2 cells. A) miR-1002 levels in heads of miR-1002 knockout, wildtype, and miR-1002 overexpression flies. Flies were fed RU486 for 5 days, then 30+ heads per N were collected for RNA extraction.Values were normalized to RP49. B) miR-1002 levels in S2 cells transfected with either a miR-1002 negative scramble plasmid or a miR-1002 overexpression plasmid. 48 hours later, RNA was extracted for RT-qPCR. Related to Figure 1, Figure 3, Figure 4, and Figure 6.

A

Drosophila NMNAT sequences

```
                                                                  miR-1002
                                                               binding sequence
                                Box 1                     Box 2
                                                               *****  *******
D. Melanogaster   5′-ACGATACGTACACTGAAT...GGTCAGTGTGCGTATCATCTACTTA-3′
D. Simulans       5′-ACGATACGTACACTGAAT...GGTCAGTGTGCGTATCATCTACTTA-3′
D. Yakuba         5′-ACGATACGTACACTGAAT...GGTCAGTGTGCGTATCATCTACTTA-3′
D. Erecta         5′-ACGATACGTACACTGAAT...GGTCAGTGTGCGTATCATCTACTTA-3′
D. Sechellia      5′-ACGATACGTACACTGAAT...GGTCAGTGTGCGTATCATCCACTTA-3′
D. Obscura        5′-CTGATACGTACACTGAAT...GGTCAGTGTACGTATCAATTACTTA-3′
D. Psuedoobscura  5′-CTGATACGTACACTGAAT...GGTCAGTGTACGTATCATTTACTTA-3′
D. Serrata        5′-CTGATACGTACACTGAAT...GGTCAGTGTGCGTATCCATCCACTT-3′
D. Ananassae      5′-TCGATACGTACACTGAGA...GGTCAGTGTGCGTATCATACAGATA-3′
D. Willistoni     5′-TTGATACGTACACTGAAC...GGTCAGTGTACGTATCACGCACCAT-3′
D. Hydei          5′-TTGATACGTACACTGAGG...TTCCAGTGTACGTATCAGCTTAGAT-3′
D. Virilis        5′-TTGATACGTACACTGATT...TTCCAGTGTACGTATCAGCTTAGGT-3′
D. Mojavensis     5′-TTGATACGTACACTGAAG...TTCCAGTGTACGTATCAGCGTAAAT-3′
D. Grimshawi      5′-TTGATACGTACACTGATG...TTCCAGTGTACGTATCATCACAAAA-3′
```

B

Drosophila miR-1002 sequences

```
                    *******  *****
D. Melanogaster   5′-UUAAGUAGUGGAUACAAAGGGCGA-3′
D. Simulans       5′-UUAAGUAGUGGAUACAAAAGGCGA-3′
D. Sechellia      5′-UUAAGUAGUGGAUACAAAAGGCGA-3′
D. Yakuba         5′-UUAAGUAGUGGAUACAAAAGGCGA-3′
D. Virilis        5′-UUAAGUAGUUAAUACAA-GGGCGA-3′
D. Erecta         5′-CUAAGUAGUGGAUACAAACGGCGA-3′
D. Pseudoobscura  5′--UAAGUAGUUGAUACAA-GGGCGA-3′
```

Figure S2- NMNAT Box 1, Box 2, miR-1002, and miR-1002's binding sequence on Box 2 are conserved across the *Drosophila* genus. A) Alignment of *NMNAT* genomic sequences for 14 *Drosophila* species. Box 1 and Box 2 nucleotides indicated on *D. Melanogaster* NMNAT. Red asterisks indicate miR-1002 binding nucleotides. B) miR-1002-5p sequence alignment for 7 Drosophila species. Red asterisks indicate *D. Melanogaster* miR-1002 nucleotides which bind to NMNAT. Data procured from miRBase, miROrtho, and FlyBase. Related to Figure 2.

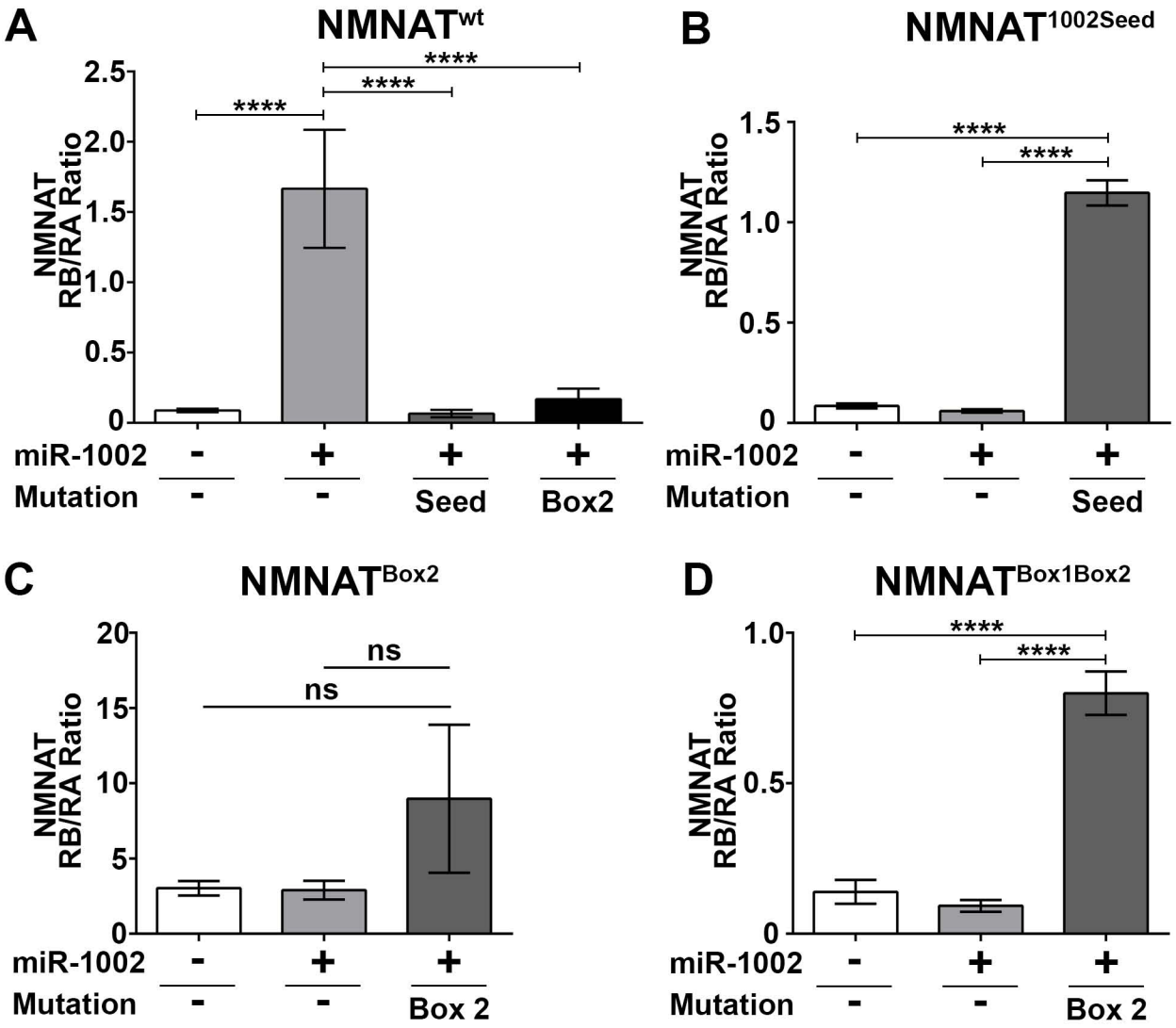

Figure S3. RB/RA ratio is significantly increased when miR-1002 can bind NMNAT reporter. A-D) S2 cells were transfected with various miR-1002 and NMNAT reporter plasmids, then RNA extracted for qPCR. Data depicted is the same as the data for Figure 3 B-E. NMNAT RB level was divided by NMNAT RA level. One-WAY NOAVA, Tukey's post hoc. ****p<.0001. N=4. Related to Figure 3.

A

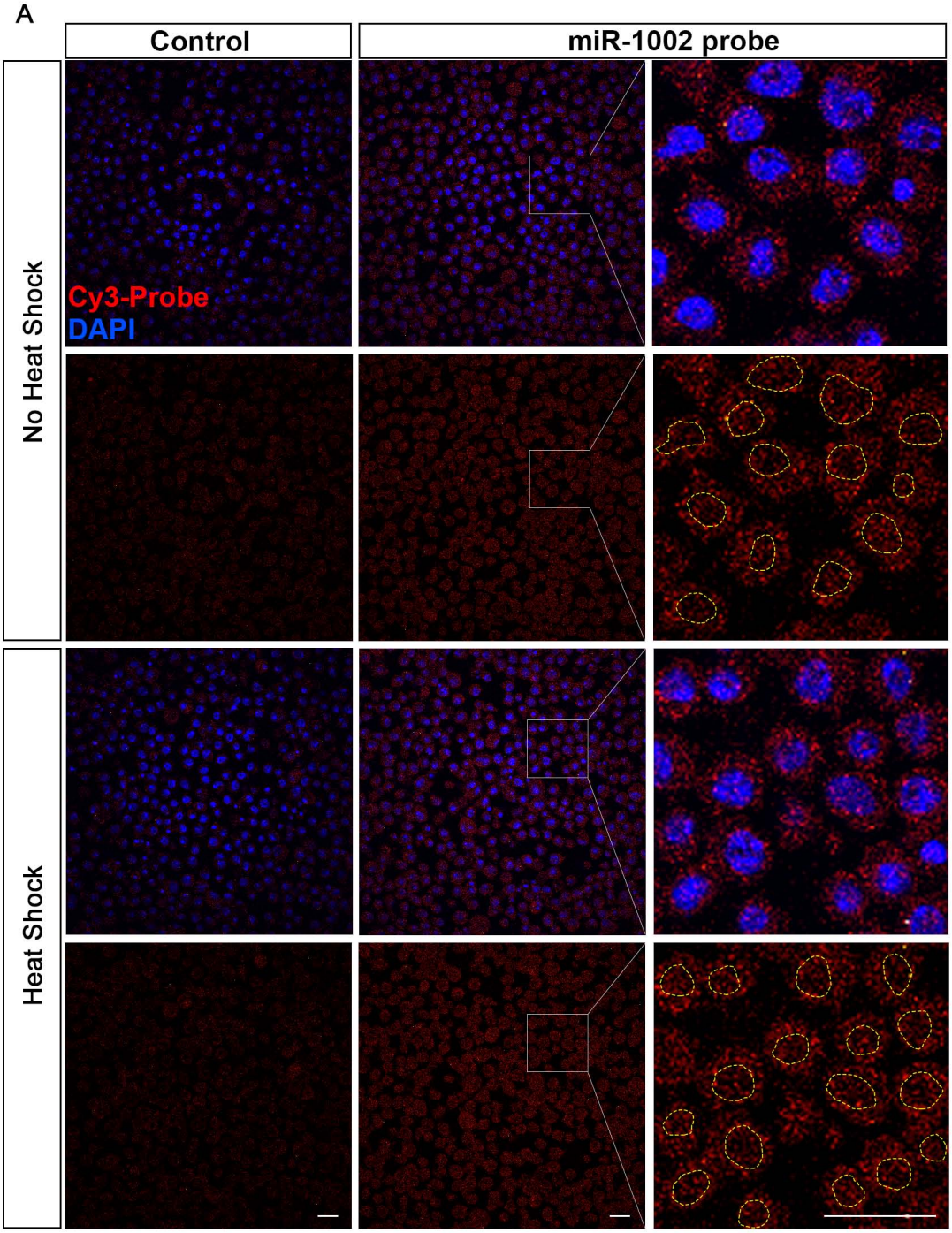
Control
miR-1002 probe
No Heat Shock
Heat Shock
Cy3-Probe
DAPI

B

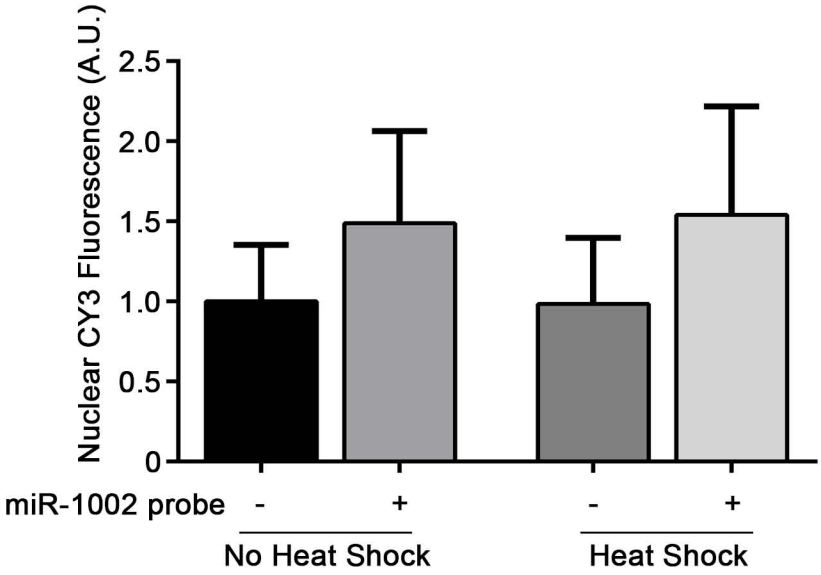
Nuclear CY3 Fluorescence (A.U.)
2.5
2.0
1.5
1.0
0.5
0
miR-1002 probe
-
+
-
+
No Heat Shock
Heat Shock

Figure S4. microRNA FISH reveals signal in nucleus of S2 Cells. A) Confocal images of S2 cells before and after heat shock, and hybridized with a probe for miR-1002 or a control probe. Nuclei were identified with DAPI staining. Yellow circles represent examples of identified nuclei. Scale bars 15 µm B) Quantification of A. Data presented as mean ± SD. N=260-411 cells. Related to Figure 6.

Supplemental Tables

Table S1. Sequences of DNA/RNA oligonucleotides and probes used in this study. Related to Figures 1, 3, 5, 6.

For Figures	Name	Sequences (From 5' to 3')
1,3,5,6	NMNAT RA FWD	TTGATTCGGCGGCTCTTAGG
1,3,5,6	NMNAT RA REV	ACCGCATCCGTTATATACTTAGATT
1,3,5,6	NMNAT RB FWD	GGCCAGTCGGTCAAGTACC
1,3,5,6	NMNAT RB REV	CGGTGCATCCCGCGATTT
1,3,5,6	RP49 FWD	CTAAGCTGTCGCACAAATGGC
1,3,5,6	RP49 REV	AACCGATGTTGGGCATCAGA
3	Luciferase FWD	GGCTTCAACGAGTACGACTTCG
3	Luciferase REV	GTACATGCTTTGGAAGCCCTGG
3	NMNAT Seed Scramble mutation FWD	GCGTATCATCTATCATCACCGAATTGTTGCC
3	NMNAT Seed Scramble mutation REV	CGGTGATGATAGATGATACGCACACTGACCACCGC
3	NMNAT Box 2 Scramble mutation FWD	GCTCTGAATCTACTTACACCGAATTGTTGCC
3	NMNAT Box 2 Scramble mutation REV	GTAGATTCAGAGCACACTGACCACCGC
3	NMNAT Box 1 Scramble mutation FWD	GTGTACTCTGAGTTTGAAAGATGGG
3	NMNAT Box 1 Scramble mutation REV	CAAACTCAGAGTACACTGAATGAGGCGCC
3	miR-1002 Seed Scramble mutation FWD	GCGGCCGCTAGAAATTATATATTATGATAGTGGATACAAAGGGC
3	miR-1002 Seed Scramble mutation REV	CCACTATCATAATATATAATTTCTAGCGGCCGCTTACTCTTTTTTTGGGTTTGGTGGGG
3	miR-1002 Box 2 Scramble mutation FWD	GTAGTGTCAGAAAAGGGCGATTTG
3	miR-1002 Box 2 Scramble mutation REV	GCCCTTTTCTGACACTACTTAAATATATAATTTCTAGCGGCCGC

6	miR-1002 FISH probe	TTAAGTAGTGGATACAAAGGGCGA
6	Control probe	TCGCCCTTTGTATCCACTACTTAA

Transparent methods

Drosophila Strains and Maintenance

Flies were maintained and crossed in a climate-regulated 25°C incubator in a 12hr light-dark schedule with 60-65% humidity on cornmeal-molasses-yeast medium. *UAS-NMNAT*$^{4-7}$ *AltReport* was previously generated in lab (Ruan et al., 2015). *yw* flies were used as wildtype controls throughout this study. Also used were *UAS-miR-1002* (Bloomington stock number 60657), *miR-1002* knockout flies (Bloomington stock number 58949), *UAS-Luciferase* (Bloomington stock number 35788), *UAS-miR-9a* (Bloomington stock number 41138), AGO1 mutant flies (Bloomington stock number 10772), and *elav-geneswitch* (Bloomington stock number 43642).

Cell Culture

Drosophila S2 cells (ATCC) were maintained at room temperature in Schneider's *Drosophila* medium (Lifetech) supplemented with 10% Fetal Bovine Serum (Atlanta Biologicals) and 1% Penicillin/Streptomycin (GIBCO). S2 cells are derived from embryonic cells and are believed to be male.

RNA Extraction and qRT-PCR

Female fly heads (30-50 per N) at 2 DAE (days after eclosion) were homogenized using a mechanical pestle homogenizer in 200µl Trizol (Sigma). After adding 800µl Trizol with 200µl chloroform and a 15min centrifugation at 4°C, the RNA layer was collected. Total RNA was extracted using Favorgen RNA mini kit according to the manufacturer's protocol. Reverse transcription was performed using the Applied Biosystems High Capacity cDNA Reverse Transcription Kit. 2 µg RNA was used in a 20 µl RT reaction according to the manufacturer's protocol. For qPCR, a 96 well plate was used. 100ng of cDNA from each sample was loaded into each well, with triplicate wells for each biological sample. Custom primers were designed for each target transcript, and Bio-Rad iQ SYBR Green Supermix added according to the manufacturer's protocol. A CFX connect real-time detection system (Bio-Rad) was used to perform qPCR. The quantification of transcripts was calculated via the 2(-Delta Delta C(T)) method (Livak and Schmittgen, 2001). RP49 was used as the reference gene. See table S1 for primer sequences.

miRNA Extraction and qRT-PCR

30+ female fly heads were collected and homogenized with a mechanical pestle homogenizer in 700 µl Qiazol reagent. After addition of chloroform and 15 min spin at 4ºC, the RNA layer was collected. Total RNA including microRNA was extracted using the miRNeasy kit (Qiagen) according to the supplier's protocol. 200 ng of RNA was used in the RT reaction with the miScript RT kit (Qiagen). qPCR was performed using a custom LNA probe for miR-1002 using the miRCury SYBR green reagent (Qiagen).

Western Blot

Female fly heads (10 per N) were collected and homogenized in RIPA buffer (Sigma). 4X SDS loading buffer was added, then samples boiled at 95ºC for 5 minutes. Samples were loaded onto a 10% SDS gel for electrophoresis. After transfer onto a nitrocellulose membrane (Biorad) and blocking with TBS/Blocking buffer (Rockland), the membrane was probed with anti-DmNMNAT (1:8,000) and anti-β-Actin antibody (1:10,000, Sigma). Membranes were further probed with dye-conjugated secondary antibodies (1:10,000, Rockland), then imaged at IR700 and IR800 on an Odyssey Infrared Imaging system (LI-COR Biosciences). Analysis was performed using Imagestudio (LI-COR).

Plasmids

pUAS-luc2 was a gift from Liqun Luo (Addgene plasmid # 24343 ; http://n2t.net/addgene:24343 ; RRID:Addgene_24343)(Potter et al., 2010). pAC-GAL4 was a gift from Liqun Luo (Addgene plasmid # 24344; http://n2t.net/addgene:24344; RRID:Addgene_24344). pRL-ubi63E was a gift from Alexander Stark (Addgene plasmid # 74280 ; http://n2t.net/addgene:74280 ; RRID:Addgene_74280) (Arnold et al., 2013). *NMNAT RB 3'UTR*, *NMNAT*$^{4\text{-}7}$, and *miR-1002* were all cloned out of *Drosophila* genomic DNA into PGEM-T-Easy before ligation into the appropriate plasmids. miR-1002 negative scramble was ordered from Genscript for ligation into pAC-GAL4.

Mutations to plasmids were created with Quikchange II site-directed mutagenesis kit (Agilent). Sequences for primers used in mutations are found in table S1.

Luciferase activity assay

Drosophila S2 cells in a 12 well plate were transfected with 3 plasmids using JetPrime- pRL-UBI-63E; pAC-GAL4-miR-1002-negativeScramble, or pAC-GAL4-miR-1002; and pUAS-LUC2-NMNAT-RB-3'UTR, or pUAS-LUC2-NMNAT-RB-3'UTR-miR-1002-seedmut. 48 hours after transfection, cells were collected and lysed with a lysing buffer (100mM KCl, 20mM HEPES, 5%

Glycerol, 0.1X Triton-X, 1mM DTT, and Complete protease inhibitor (Roche)). ProMega DUAL-GLO Luciferase assay was performed to measure firefly and Renilla luciferase activity according to the manufacturer's protocols. Luminescence was measured using a FluoStar Omega microplate reader in a 96 well plate, with triplicate wells per biological sample.

Actinomycin D chase assay

Actinomycin D (Sigma) was reconstituted in DMSO (Sigma) at a concentration of 1mg/ml. S2 cells were transfected with pAC-GAL4-miR-1002 or pAC-GAL4-miR-1002-scramble. 48 hours after transfection, Actinomycin D was added to the cells at a concentration of 10 µg/ml. Cells were harvested at 0, 1, 2, and 3 hours after actinomycin treatment, then RNA collected for qPCR.

Minimum Free Energy (MFE) RNA secondary structures

RNA secondary structures were predicted using RNAfold as of the Vienna RNA package. Secondary structures were visualized using the FORNA web server (http://rna.tbi.univie.ac.at/forna/). *Nmnat* exon 4-intron 5 and the various mutations (Figures 3A, 3C-E) were modelled for MFE through Vienna RNA fold (Lorenz et al., 2011). The structure was then visualized using FORNA (Kerpedjiev et al., 2015). miR-1002 was manually inserted in Figure 3B. RNAStructure's duplexfold function was used to calculate MFE values (Reuter and Mathews, 2010).

Drug feeding

RU486 (mifepristone, Sigma) was dissolved in ethanol, then mixed into fly food at a concentration of 50µg/ml. Flies expressing an elav geneswitch driver were fed food containing drugs or vehicle control for 5 days before brains were dissected.

Immunocytochemistry of fly brains

Adult female brains were fixed in 3.5% formaldehyde for 15 min and washed in PBS with 0.4% Triton X-100. Brains were incubated with anti-RFP (Abcam, 1:500) and an alexa-555 conjugated secondary antibody (Invitrogen, 1:250). DAPI (Invitrogen, 1:300) staining was performed post-secondary antibody staining. All antibody incubations were performed at 4 °C overnight in the presence of 5% normal goat serum. Brains were then mounted and imaged on an Olympus IX81 confocal microscope and processed using FluoView 10-ASW (Olympus). Images were quantified using ImageJ. The midbrains of 3 brains per genotype were analyzed.

Stress Paradigms

For heat stress, female flies were collected 2 DAE and subjected to a 15 or 45-minute heat shock in vials placed into a 37ºC incubator. Flies were collected after heat shock for RNA extraction from heads.

For thermotolerance assay, 20 flies per vial at 2 DAE were submerged in a 35ºC water bath for a 30-minute preconditioning. Flies were immediately moved to a 39ºC water bath. Vials were checked under a light microscope every 10 minutes to count paralyzed flies.

Subcellular Fractionation

S2 cells were collected and washed in ice cold PBS. Subcellular fractionation was performed with the NE-PER kit (Thermo-Fisher), according to the manufacturer's instructions. Both nuclei and cytoplasmic fractions were collected. Western blot was performed for AGO1 (abcam), α-Tubulin (Sigma), Calreticulin (Abcam) and Histone-H1 (active motif).

Confocal image acquisition and processing

Confocal microscopy was performed with an Olympus IX81 confocal microscope and processed using FluoView 10-ASW (Olympus) and Adobe Photoshop CS6 (Adobe Systems, San Jose, CA, USA).

S2 cell immunostaining

Coverslips were treated with 20 ug/ml of poly-D-lysine in Hank's Basic Salt Solution on 35-mm culture dishes overnight. Coverslips were rinsed with S2 cell medium before seeding cells. 24 hours post seeding, heat shock the cells at 37ºC for 1 h. Cells were fixed with 4% formaldehyde for 15 min and permeabilized with 0.4% Triton X-100 for 5 min. Coverslips were blocked with 5% goat serum in PBS at 37ºC for 30 min and then incubated with AGO1 antibody (1:100) in blocking solution at 37ºC for 2 h. After washing with PBS for 5 min, 3 times, coverslips were incubated with Cy5-labeled anti-rabbit secondary antibody (1:500) in blocking solution at 37ºC for 1 h. In the second PBS wash, DAPI was added (1:10000), then coverslips mounted with VECTASHIELD Antifade Mounting Medium.

Quantification of nuclear AGO1 was performed as previously described (Brazill et al., 2018). Briefly, images were taken using a 60x oil immersion objective lens. Region of interest (ROI) was selected based on DAPI staining. Auto-segmentation was conducted by interactive h-maxima watershed. Three parameters were adjusted: seed dynamics determined by h-maxima

(h=5892), global watershed stop criteria determined by intensity threshold (T=1119), and regional stop criteria determined by peak flooding (%=90). Nuclei were defined as objects larger than 10 μm^2.

Florescence in situ hybridization

Coverslips were incubated with 20 ug/ml poly-D-lysin (stock concentration: 1 mg/ml, 1:50) in HBSS in a 35-mm cell culture dish (at least 1.5 ml for each dish) at room temperature overnight. After the coating solution was removed and the coverslip washed with 1 ml of prewarmed culture medium, cells were seeded with at 50% confluence.

16-24 h post seeding, cells were heat shocked at 37°C for 1 h. The media was removed and cells were fixed with 4% formaldehyde in PBS for 30 min at room temperature. After washing with PBS, cells were permeabilized with 0.2 M HCl for 30 min at room temperature. Cells were washed with PBS, then rehydrated for 5 minutes at room temperature with 1.5 ml of 2x SSC (300 mM NaCl, 30 mM sodium citrate, pH 7.0), 50% formamide. Cells were hybridized overnight at 37°C in 40 µl of a mixture containing 10% dextran sulfate, 2 mM vanadyl-ribonucleoside complex, 2x SSC, 50% formamide, 100 ng of probe (denatured at 85 degree for 10 min). Cells are washed twice for 15 min with 1.5 ml of 2x SSC, 50% formamide at room temperature, then incubated with DAPI solution (1:10000 in PBS) for 5 min at room temperature. They were washed a final time in PBS before imaging.

Quantification and Statistical Analysis

Prism was used for statistical analysis and graph generation. Student's t-test, one-way ANOVA, and two-way ANOVA with Tukey's post hoc were used. Log-rank test was used to calculate significant differences between the 2 populations in the thermotolerance assay. All analyses were two-tailed. *$p<0.05$, **$p<0.01$, ***$p<0.001$, ****$p<0.0001$

Data and Software Availability

Putative microRNA seed sequence scan was performed using (http://microRNA.org) (Betel et al., 2008, 2010; Enright et al., 2003; John et al., 2004). RNA secondary structures were modelled using RNAfold as of the Vienna RNA package (Lorenz et al., 2011). Secondary structures thus obtained were visualized using web-based FORNA (http://rna.tbi.univie.ac.at/forna/) (Kerpedjiev et al., 2015). RNA duplex minimum free energy values were calculated using RNAStructure (Reuter and Mathews, 2010).

Supplemental References

Arnold, C.D., Gerlach, D., Stelzer, C., Boryń, Ł.M., Rath, M., and Stark, A. (2013). Genome-wide quantitative enhancer activity maps identified by STARR-seq. Science *339*, 1074–1077.

Betel, D., Wilson, M., Gabow, A., Marks, D.S., and Sander, C. (2008). The microRNA.org resource: targets and expression. Nucleic Acids Res. *36*, D149-153.

Betel, D., Koppal, A., Agius, P., Sander, C., and Leslie, C. (2010). Comprehensive modeling of microRNA targets predicts functional non-conserved and non-canonical sites. Genome Biol *11*, R90.

Brazill, J.M., Zhu, Y., Li, C., and Zhai, R.G. (2018). Quantitative Cell Biology of Neurodegeneration in Drosophila Through Unbiased Analysis of Fluorescently Tagged Proteins Using ImageJ. J Vis Exp.

Enright, A.J., John, B., Gaul, U., Tuschl, T., Sander, C., and Marks, D.S. (2003). MicroRNA targets in Drosophila. Genome Biol. *5*, R1.

John, B., Enright, A.J., Aravin, A., Tuschl, T., Sander, C., and Marks, D.S. (2004). Human MicroRNA targets. PLoS Biol. *2*, e363.

Kerpedjiev, P., Hammer, S., and Hofacker, I.L. (2015). Forna (force-directed RNA): Simple and effective online RNA secondary structure diagrams. Bioinformatics *31*, 3377–3379.

Livak, K.J., and Schmittgen, T.D. (2001). Analysis of relative gene expression data using real-time quantitative PCR and the 2(-Delta Delta C(T)) Method. Methods *25*, 402–408.

Lorenz, R., Bernhart, S.H., Höner Zu Siederdissen, C., Tafer, H., Flamm, C., Stadler, P.F., and Hofacker, I.L. (2011). ViennaRNA Package 2.0. Algorithms Mol Biol *6*, 26.

Potter, C.J., Tasic, B., Russler, E.V., Liang, L., and Luo, L. (2010). The Q system: a repressible binary system for transgene expression, lineage tracing, and mosaic analysis. Cell *141*, 536–548.

Reuter, J.S., and Mathews, D.H. (2010). RNAstructure: software for RNA secondary structure prediction and analysis. BMC Bioinformatics *11*, 129.

Ruan, K., Zhu, Y., Li, C., Brazill, J.M., and Zhai, R.G. (2015). Alternative splicing of Drosophila Nmnat functions as a switch to enhance neuroprotection under stress. Nat Commun *6*, 10057.

Zuker, M., and Stiegler, P. (1981). Optimal computer folding of large RNA sequences using thermodynamics and auxiliary information. Nucleic Acids Res. *9*, 133–148.